Two Robust Multivariate Exponentially Weighted Moving Average Charts to Facilitate Component Wise Assessment

Abstract

This paper offers new multivariate statistical process monitoring schemes to study the process shift supported by a component-wise assessment. The proposed procedures help determine whether one or more features have undergone a shift or whether the shift is in the dependence structure but not in the study variables. We use the marginal distributions and pseudo copula observations to effectively apply component-wise rank-based Lepage and Cucconi tests. The rank-based statistics induce nonparametric properties to the proposed chart. Therefore, its in-control performance is highly robust and nearly distribution-free. It is shown that the new chart gives better results for detecting scale shifts in one or more quality variables than some representative existing nonparametric charts. Some Monte-Carlo simulation studies have been performed to establish the effectiveness of the new charting scheme. A real application involving the production quality of cork stoppers is considered to illustrate the use of the proposed schemes in manufacturing and production. Some encouraging component-wise assessment properties are observed.

Keywords: Cucconi statistic; Lepage statistic; Multivariate processes; Principal component score; Pseudo copula; Statistical process control.

1 Introduction

In monitoring the stability of a process, statistical process monitoring (SPM) plays an essential role (Qiu 2014). Data variation in process observations can be due to random noise (called common-cause variation) or attributable to a particular cause (called special-cause variation). Understanding the source of data variation through process monitoring is essential to guarantee the stability of a process. SPM charts are explicitly designed to distinguish special causes of variation from common causes. The actual reasons for special causes of variation can be figured out promptly once an SPM chart detects the special causes of variation. In addition, they are easy to implement with visual presentations. Thus, they provide an effective and convenient tool for the sequential monitoring of process data over time. It should be pointed out that early SPM charts were developed mainly for monitoring industrial production lines (Shewhart 1931). In recent years, they have been used in many other applications, including quality management of cab services (Song, Mukherjee, and Tao 2020), call centre services (Mukherjee and Marozzi 2017), and post-sales online review processes (Zhang, He, Zhao, and Qu 2021).

Consider the problem of monitoring cork stoppers or piston rings where one needs to monitor length and diameter simultaneously. The two quality characteristics are often correlated. Similarly, in cab services, the waiting time, the trip duration, and the trip distances are often recorded daily to monitor service quality.

Here also, quality characteristics are often found correlated. Thus joint monitoring of several quality characteristics simultaneously should be considered, and it comes under the multivariate SPM problem in the literature (Qiu 2014, Chapters 7 and 9). In the multivariate SPM literature, traditional methods assume that the joint distribution of several quality characteristics has a known parametric distribution (e.g., multivariate Gaussian distribution). Then, control charts based on Hotelling's T^2 statistic are popular. However, such a multivariate parametric distribution assumption is often invalid in practice. Various literature has demonstrated that control charts based on this assumption would be unreliable when the assumption is invalid (e.g., Qiu and Hawkins 2001). Some nonparametric SPM methods have been developed to overcome this limitation. See, for instance, Qiu and Hawkins (2001, 2003), Qiu (2008), Liu, Tsung and Zhang (2014), Qiu and Zhang (2015), Li, Jeske, Zhou, and Zhang (2019), and Hou and Yu (2020). For recent overviews on multivariate SPM, see Qiu (2018) and Chakraborti and Graham (2019).

In recent years, Qiu (2020) introduced some contemporary SPM methods and discussed their potential in many big data applications. Mukherjee and Marozzi (2020) designed some Shewhart-type nonparametric schemes to monitor multiple quality characteristics based on specific distance metrics. Xue and Qiu (2021) developed a nonparametric CUSUM scheme for monitoring multivariate serially correlated processes. Song, Mukherjee, and Zhang (2021) proposed two adaptive approaches for detecting the signal source in a bivariate process. In addition, the machine learning algorithm, including dimension reduction tools such as principal component analysis, has emerged as a powerful tool that can be integrated with SPM control charts to deal with massive data from a continuous process. Interested readers can see the book Tran (2022) for an excellent survey and the paper by Qiu and Xue (2021) for a recent methodology. For some earlier works, see, for instance, Zou, Wang, and Tsung (2012), Li, Zou, Wang, and Huwang (2013), and Chen, Zi, and Zou (2016).

One necessary property for a multivariate monitoring scheme to be helpful in an application is its effectiveness in accurately locating the source of assignable causes when a shift is detected. However, in multidimensional cases, identifying the signal source or variables responsible for the shifts is often more complex. Since several mutually correlated quality characteristics are involved in multivariate cases, it is often hard to figure out which ones cause the shift. There is still a lack of available diagnostic methods that can offer exhaustive diagnostic information when a multivariate process is declared out of control (OOC). To overcome this difficulty, Song, Mukherjee, and Zhang (2021) developed some adaptive SPM procedures for identifying the signal source in a bivariate process after a shift is detected in the location vector, the scale matrix, or both. Their method capitalised on Sklar's principle that any multivariate joint distribution function can be written using univariate marginal distribution functions and a copula. The copula describes the dependence structure among different quality characteristics.

The control charts described in Song, Mukherjee, and Zhang (2021) are Shewhart charts and are limited to bivariate cases. Each plotting statistic of their proposed charts comprises three component statistics: two statistics respectively for the two marginal process distributions and one for the copula to monitor dependence structure. Their proposed charting statistic directly computed the Lepage or Cucconi statistic and corresponding p-values to compare the marginal process distributions. Song, Mukherjee, and Zhang (2021) used a Euclidean Distance based statistic to monitor the equality of two empirical copulas. It computed the Euclidean distance of pseudo-observations of the reference sample and a test sample from the origin (0,0) as the reference and test copula distance sample. Subsequently, the Lepage or Cucconi statistics and corresponding p-values are computed based on the reference and test copula distances.

The control charts described in Song, Mukherjee, and Zhang (2021) are Shewhart charts. Consequently, they are less sensitive to small and persistent shifts. Apart from that, there are two other limitations of this method. First, the pseudo-observations of the copula are correlated, and the corresponding p-value does not follow a Uniform distribution in the interval (0,1). Moreover, when the test sample size is small, a typical case in SPM applications, the method is not sensitive enough to detect correlation shifts. This paper monitors the marginal distributions and the copula function simultaneously, as in Song, Mukherjee, and Zhang (2021). However, unlike them, it proposes some exponentially weighted moving average (EWMA) monitoring schemes to detect if there is any change in the multivariate processes. Intuitively, EWMA charts would be more effective than the Shewhart charts for detecting small to moderate shifts (cf., Qiu 2014, Chapters 5 and 7). Further, while we consider the same approach, as in Song, Mukherjee, and Zhang (2021), for developing the component statistics for monitoring marginal distributions, the component statistic for monitoring copula (dependence structure) is very different in the current context.

This paper suggests a better and more powerful statistic for monitoring the equality of copula using eigenvalues. Therefore, the current proposal uses a multivariate EWMA (MEWMA) setup and employs a different (and new) plotting statistic for the dependence component. The new approach for the dependence structure considers the pseudo copula observations of the combined reference sample and a test sample and subsequently computes the principal component scores (PCS). The maximum of the Lepage or Cucconi statistic for test and reference PCS is computed to detect pseudo-copula changes, ensuring the corresponding p-value follows uniform distribution in the interval (0,1). The simulation results show that the modified multivariate charts perform much better in detecting pure downward correlation shifts, despite the small test sample size.

The following describes the outline of the remaining paper. Section 2 presents our model framework and some statistical test procedures. Section 3 summarises the implementation steps and related algorithms of the proposed multivariate EWMA monitoring schemes. Section 4 is devoted to introducing a review of some representative existing nonparametric charts. We carry out a detailed performance analysis using Monte Carlo in Section 5. Section 6 presents a real data example to show the implementation of newly designed schemes. We offer a summary and some concluding remarks in Section 7.

2 Statistical Framework

Consider any d-dimensional cumulative distribution function (CDF) F^d and a random vector $\boldsymbol{V} = (V_1, V_2, \ldots, V_d)$ having joint distribution F^d with continuous marginal CDFs $F_1, F_2, \ldots, F_d$. Sklar (1959) presented that the d-variate CDF F^d of $\boldsymbol{V}$ can be uniquely written in the form:

$$F^d(v_1, v_2, \ldots, v_d) = C\{F_1(v_1), F_2(v_2), \ldots, F_d(v_d)\},$$

where C is a distinctive copula function defined as the joint CDF of $F_1, F_2, \ldots, F_d$. Note that C holds all information on the dependence structure between the components of $\boldsymbol{V}$ whereas the marginal CDFs $F_1, F_2, \ldots, F_d$ encompass all information on the marginal distributions.

Sklar's theorem clarifies how any multivariate joint distribution can be expressed via its univariate marginal distribution functions and copula. Consequently, we can effectively monitor a multivariate process by conveniently monitoring each marginal distribution and the copula function. Unlike the

parametric procedures, we need not elucidate the distribution types and estimate the distribution parameters in advance but require a Phase-I data set from an in-control (IC) process as the reference sample in the monitoring schemes. To this end, we suppose the subsequent model framework. Let $\boldsymbol{\Psi_{0m}} = \{(X_{10i}, X_{20i}, \cdots, X_{d0i}),\ \ i = 1, 2, \cdots, m\}$ be a set of m reference sample observations from a d-variate IC process with a continuous but unknown CDF $F_0 \equiv F_0(x_1, x_2, \cdots, x_d)$. It is worth noting that one needs to establish a reference sample through a suitable Phase-I analysis. To establish a Phase-I sample, see Jones-Farmer, Woodall, Steiner, and Champ (2014) and Capizzi and Masarotto (2018). Suppose $\boldsymbol{\Psi_{jn}} = \left\{(X_{1ji'}, X_{2ji'}, \cdots, X_{dji'}),\ \ i' = 1, 2, \cdots, n\right\}$ be the j^{th} $(j = 1, 2, \ldots)$ test sample of size n, collected successively during the Phase-II monitoring, from a CDF $F_1 \equiv F_1(x_1, x_2, \cdots, x_d)$. A test sample is mutually independent of the reference sample. Ideally, two CDFs F_0 and F_1 should be identical in all aspects when the process is IC. Therefore, the monitoring problem can be transformed into the following hypothesis:

$$H_0: \quad F_0(x_1, x_2, \cdots, x_d) = F_1(x_1, x_2, \cdots, x_d); \qquad H_1: \quad F_0(x_1, x_2, \cdots, x_d) \neq F_1(x_1, x_2, \cdots, x_d)$$

Suppose that $F_{p0}(x)$ and $F_{p1}(x)$, $p = 1, 2, \cdots, d$ are the d continuous marginal CDFs of F_0 and F_1, respectively. According to Sklar's theorem, $F_0(x_1, x_2, \cdots, x_d) = C_0\{F_{10}(x_1), F_{20}(x_2), \cdots, F_{d0}(x_d)\}$, and $F_1(x_1, x_2, \cdots, x_d) = C_1\{F_{11}(x_1), F_{21}(x_2), \cdots, F_{d1}(x_d)\}$. Using Sklar's theorem, it is easy to see that the equivalence of joint distributions F_0 and F_1 can be established by testing the equivalence of marginal distributions F_{p0} and F_{p1} for $p = 1, 2, \cdots, d$ as well as the copula functions $C_0(\cdot)$ and $C_1(\cdot)$. Therefore, one may equivalently test the H_0 by jointly evaluating $d + 1$ hypotheses, say, $H_{0p}: F_{p0}(x) = F_{p1}(x), \quad p = 1, 2, \cdots, d, \quad$ and $\quad H_{00}: C_0(x_1, x_2, \cdots, x_d) = C_1(x_1, x_2, \cdots, x_d)$. When the process is OOC, at least one of the $H_{0p'}, \quad p' = 0, 1, \cdots, d$ is violated.

Motivated by this, Song, Mukherjee and Zhang (2021) developed two Shewhart-type procedures, denoted as the Lepage-Copula and Cucconi-Copula schemes, based on the p-values of three nonparametric tests, two for the equality of individual marginal distributions and the other for equality of two copulas. However, they restricted themselves to $d = 2$ only and Shewhart-type charts. In this paper, we propose two MEWMA-type schemes for monitoring multivariate processes. We also modify the component test statistic for copula. In the subsequent subsections, we introduce several relevant test procedures.

2.1 The Lepage and Cucconi tests statistics

Marozzi (2013) showed that the Lepage and Cucconi statistics perform well for various distributions in testing location-scale problems. The Lepage test is the sum of squares of two standardised statistics: the Wilcoxon rank-sum (WRS) statistic for location and the Ansari-Bradley (AB) statistic for scale. On the other hand, Nishino and Murakami (2019) established that the Cucconi statistic is half the sum of squares of two standardised statistics: the WRS statistic for location and the Mood (MD) statistic for scale. Song, Mukherjee, Marozzi, and Zhang (2020) gave three possible representations of the Cucconi statistic as a quadratic combination of two orthogonal statistics. We use the most straightforward form offered by Nishino and Murakami (2019).

Let $\{U_i | i = 1, 2, \ldots, m\}$ be the reference sample of size m, drawn from univariate distribution G_U. Let $\{W_{i'} | i' = 1, 2, \ldots, n\}$ be the test sample of size n, collected from univariate population $G_W = G_U\left(\frac{x-\theta}{\delta}\right)$. Here, $-\infty < \theta < +\infty$, $\delta > 0$, are the unknown location and scale parameters, respectively. We further assume that the test sample is mutually independent of the reference sample. Combining the reference and

test samples and arranging all $N = m + n$ observations in ascending order, the rank of W's can be denoted by $R_k, k = 1, 2, .., n$. The WRS, AB and MD statistics are respectively given by:

$$T_W = \sum_{k=1}^{n} R_k, \qquad T_{AB} = \sum_{k=1}^{n} \left| \frac{N+1}{2} - R_k \right| \qquad \text{and} \qquad T_{MD} = \sum_{k=1}^{n} \left(\frac{N+1}{2} - R_k \right)^2.$$

The Lepage and Cucconi statistics are, respectively, given by

$$L = \left(\frac{T_W - \mu_{T_W}}{\sigma_{T_W}} \right)^2 + \left(\frac{T_{AB} - \mu_{T_{AB}}}{\sigma_{T_{AB}}} \right)^2, \tag{1}$$

and

$$C = \frac{1}{2} \left[\left(\frac{T_W - \mu_{T_W}}{\sigma_{T_W}} \right)^2 + \left(\frac{T_{MD} - \mu_{T_{MD}}}{\sigma_{T_{MD}}} \right)^2 \right]. \tag{2}$$

Here μ_{T_*} and σ_{T_*} are, respectively, the mean and standard deviations of the corresponding statistic. These expressions, along with references, can be found in Song, Mukherjee, Marozzi, and Zhang(2020). It is easy to see that $E(L|\text{IC}) = 2$, and $E(C|\text{IC}) = 1$. Further, irrespective of the type and the direction of the shift, $E(L|\text{OOC}) > 2$ and $E(C|\text{OOC}) > 1$. Consequently, a one-sided scheme based on the Lepage or Cucconi statistic is desired to detect a shift in any direction.

In an interesting development, Li and Qiu (2014) proposed dynamic nonparametric monitoring via the p-value method in detecting the location shift of a process. They argued that there are several benefits of employing the p-value approach. Motivated by this, Chong, Mukherjee, and Khoo (2019) developed three distribution-free schemes using different combining metrics for the p-values. They considered joint monitoring of the process location and scale parameters in a univariate setup. Furthermore, Song, Mukherjee, and Zhang (2021) proposed two adaptive procedures for monitoring bivariate processes by combining appropriate transforms of the three p-values of the component testing. In the line of Song, Mukherjee, and Zhang (2021), for both the Lepage and Cucconi statistics, the permutation-based upper one-sided p-value formula is given by

$$\text{p-value} = \frac{\text{Number of test statistic} \geq \text{observed test statistic}}{\binom{m+n}{m}}.$$

Note that if $\binom{m+n}{n}$ is large, the total number of permutations increases exponentially. To avoid this, we suggest adopting 10000 randomly selected permutations to calculate the p-values of the Lepage or Cucconi statistics, as the case may be.

For monitoring a deviation in either location or scale or both in any of the marginal distributions during Phase-II, we consider a traditional location-scale model given by $F_{p1}(x) = F_{p0}\left(\frac{x-\theta_p}{\delta_p}\right)$, $p = 1, 2, \cdots, d$. $-\infty < \theta_p < +\infty$, $\delta_p > 0$, where the constants θ_p and δ_p stand for the unknown location and scale parameters of the p^{th} marginal distribution, respectively. The marginal distribution, but not the entire process, is considered IC when $\theta_p = 0$ and $\delta_p = 1$ for $p = 1, 2, \cdots, d$. Suppose that, $\mathbf{0_d}$ and $\mathbf{1_d}$ are the d-dimensional vectors of 0's and 1's, respectively. Note that $(\theta_1, \theta_2, \cdots, \theta_d) \neq \mathbf{0_d}$ and $(\delta_1, \delta_2, \cdots, \delta_d) = \mathbf{1_d}$, indicates a pure shift in the location vector; whereas $(\theta_1, \theta_2, \cdots, \theta_d) = \mathbf{0_d}$ and $(\delta_1, \delta_2, \cdots, \delta_d) \neq \mathbf{1_d}$, represents only a shift in the diagonals of the scale matrix.

For any given p and at any stage j, identify, $\{X_{p0i} | i = 1, 2, \ldots, m\}$ with U_i's and $\{X_{pji'} | i' = 1, 2, \ldots, n\}$ with V_i's. Subsequently, using Equations (1) and (2), we obtain Lepage and Cucconi statistics for the p^{th} marginal distribution as L_{pj} and C_{pj} for testing the hypothesis H_{0p}. The correlation shift is indicated by

testing H_{00} and will be discussed in the next subsection. Although originally developed only to test the joint location-scale problems, both Lepage and Cucconi statistics appear to be highly efficient in testing more general alternatives. See, for example, Marozzi (2019). Therefore, the proposed schemes are equally applicable if the location-scale for $F_{p1}(x)$ is violated.

2.2 Testing equality of the two empirical copulas

The copula is popularised in multivariate statistical approaches as it allows practitioners to model the joint distributions of random vectors separately by evaluating marginal CDFs and the copula function. However, most existing copula methods in the literature are parametric, and their functional forms relate to the underlying distributions. We use the pseudo-observations based on ranks corresponding to empirical copula to circumvent this problem and design a robust monitoring procedure.

Let $\boldsymbol{\Gamma_j}$ be the matrix of pseudo observations corresponding to empirical copula of $\{\boldsymbol{\Psi_{0m}}, \boldsymbol{\Psi_{jn}}\}$, the combined reference sample and j^{th} test sample, as a matrix size $(m+n) \times d$. Note that it is straightforward with the R code *pobs* of the package *copula*. The p^{th} column of $\boldsymbol{\Gamma_j}$ is given by $\left(\frac{R_{p01}}{m+n+1}, \cdots, \frac{R_{p0m}}{m+n+1}, \frac{R_{pj1}}{m+n+1}, \cdots, \frac{R_{pjn}}{m+n+1},\right)$, where R_{p0i} and $R_{pji'}$ are, respectively, the ranks of X_{p0i} and $X_{pji'}$ in the combined vector $\{X_{p01}, \cdots, X_{p0m}, X_{pj1}, \cdots, X_{pjn}\}$ for any p. That is, in the case of no ties in any of the coordinate samples, the pseudo-observations can be calculated component-wise by applying the marginal empirical distribution functions to the data and scaling the results by $\frac{m+n}{m+n+1}$. The scaling factor is asymptotically negligible. It ensures that the pseudo observations fall inside the open unit hypercube. The adjustment has some practical advantages, for example, avoiding density evaluation problems at the boundaries. When there are ties in the observations, we may use random allocations in tied places.

Suppose that $\boldsymbol{\Theta_j}$ be a $(m+n) \times d$ matrix of PCS corresponding to $\boldsymbol{\Gamma_j}$, and d columns of $\boldsymbol{\Theta_j}$ are linearly independent of each other. Let $\boldsymbol{Z_l} = (\xi_{p01[j]}, \ldots, \xi_{p0m[j]}, \xi_{pj1}, \ldots, \xi_{pjn})$ be the p^{th} column of $\boldsymbol{\Theta_j}$, $p = 1, 2, \ldots, d; \quad j = 1, 2, \ldots$. We have noted earlier that a shift in the dependence structure of F_0 to F_1 is expected to be captured by testing H_{00}. Intuitively, it can be verified through the structural difference in the distribution of $\{\xi_{p0i[j]} | i = 1, 2, \ldots, m\}$ and $\{\xi_{pji'} | i' = 1, 2, \ldots, n\}$. In case, $C_0(\cdot) = C_1(\cdot)$, naturally the parent distribution of $\{\xi_{p0i[j]}\}$ and $\{\xi_{pji'}\}$ are also identical for all p $(p = 1, 2, \ldots, d)$.

Identifying $\{\xi_{p0i[j]}\}$ with U_i's and $\{\xi_{pji'}\}$ with $W_{i'}$'s, we compute the Lepage statistic L_{p0j} and the Cucconi statistic C_{p0j} at the j^{th} stage of inspection, for joint monitoring of the location and scale parameters of the parent distributions of $\{\xi_{p0i[j]}\}$ and $\{\xi_{pji'}\}$ using Equations (1) and (2). We can obtain d such Lepage or Cucconi statistics for d columns of the $\boldsymbol{\Theta_j}$, and define the pivot statistic

$$L_{0j} = \max\{L_{10j}, L_{20j}, \ldots, L_{d0j}\}. \tag{3}$$

Similarly, the pivot statistic based on Cucconi is given by

$$C_{0j} = \max\{C_{10j}, C_{20j}, \ldots, C_{d0j}\}. \tag{4}$$

In the next section, we shall discuss the model construction of EWMA-type monitoring schemes based on combining appropriate transforms of the $d+1$ p-values of the component testing.

3 Design and implementation of the MEWMA-LC and MEWMA-CC scheme

Inspired by the wide use of p-value approaches in hypothesis testing in business and industry, we develop two MEWMA plotting statistics, denoted as the MEWMA-Lepage-Copula (MEWMA-LC) and the MEWMA-Cucconi-Copula (MEWMA-CC). To this end, we consider $d+1$ p-values, d p-values for testing the equality of d marginal distributions separately, and the $(d+1)^{\text{th}}$ for testing the equality of dependence structures between the variables. Now we provide the detailed implementation steps of the proposed MEWMA-LC and MEWMA-CC schemes based on Tippett's combining function to combine the p-values.

Step 1: Collect a Phase-I sample of size m from an IC process and establish it as a reference sample $\boldsymbol{\Psi_{0m}}$ using Phase-I analysis.

Step 2: Inspect a batch of test samples of size n sequentially and set the j^{th} test sample as $\boldsymbol{\Psi_{jn}}$, $j = 1, 2, \ldots$.

Step 3: At any stage $j = 1, 2, \ldots$, and for any $p = 1, 2, \ldots d$, calculate the p-values for testing H_{p0} of equality of the p^{th} marginal distributions in reference and test samples against H_{p1} following discussions of subsection 2.1. That is, obtain the p-values:
A. $\{P_{L_{pj}}\}$ using the Lepage statistic L_{pj} for the MEWMA-LC scheme;
B. $\{P_{C_{pj}}\}$ using the Cucconi statistic C_{pj} for the MEWMA-CC scheme.

Step 4: Compute the PCS matrix of pseudo-observation corresponding to empirical copula as $\boldsymbol{\Theta_j}$ following the discussion of subsection 2.2 for testing H_{00}, the equality of dependence structure against H_{01}. Precisely, obtain:
A. the Lepage statistic L_{0j} as in Equation (3) and corresponding p-value, say $\{P_{L_{0j}}\}$ for the MEWMA-LC scheme;
B. the Cucconi statistic C_{0j} as in Equation (4) and corresponding p-value, say $\{P_{C_{0j}}\}$ for the MEWMA-CC scheme.

Step 5: A. Construct the MEWMA-LC plotting statistic in the following way. Define,

$$E_{L,p',j} = \lambda \left(-\ln P_{L_{p'j}} - 1\right) + (1-\lambda)\, E_{L,p',j-1}, \quad p' = 0, 1, \ldots, d,$$

where λ is the smoothing parameter, ln stands for natural logarithm. With some elementary probability calculus, for large samples and regularity, one can obtain $E\left(-\ln P_{L_{p'j}} | \text{IC}\right) = 1$. Consequently, the starting value is taken as $E_{L,p',j}$ may be set to 0. That is, $E_{L,p',0} = 0$. Then, we can define and compute the j^{th} MEWMA-LC plotting statistic as

$$ELC_j = \max\{E_{L,p',j} | p' = 0, 1, 2, \ldots, d\}.$$

B. Construct the MEWMA-CC plotting statistic in the following way. Define,

$$E_{C,p',j} = \lambda \left(-\ln P_{C_{p'j}} - 1\right) + (1-\lambda)\, E_{C,p',j-1}, \quad p' = 0, 1, \ldots, d,$$

where λ and ln carry similar meaning as above. Also, by similar argument as above $E\left(-\ln P_{C_{p'j}} | \text{IC}\right) = 1$, and $E_{C,p',0} = 0$. Subsequently, we can define and compute the j^{th} MEWMA-CC plotting statistic

as

$$ECC_j = \max\{E_{C,p',j} | p' = 0, 1, 2, \ldots, d\}.$$

Step 6: At the j^{th} stage of monitoring plot:
A. the observed value of the statistic ELC_j against H_L, for the MEWMA-LC scheme;
B. the observed value of the statistic ECC_j against H_C, for the MEWMA-CC scheme.
Here H_L and H_C are the upper control limit (UCL) corresponding to the MEWMA-LC and MEWMA-CC schemes, respectively. Determination of H_L and H_C are deferred to the subsequent subsection.

Step 7: We obtain an OOC signal at the j^{th} test sample if:
A. $ELC_j > H_L$, for the MEWMA-LC scheme;
B. $ECC_j > H_C$, for the MEWMA-CC scheme.
Subsequently, a follow-up procedure for searching assignable causes begins. Otherwise, the process is considered IC and the inspection is continued.

Step 8: A systematic and thorough examination of signals following an alarm is critical in multivariate SPM. Identifying the OOC components is difficult with most traditional multivariate SPM schemes. Our proposed schemes are very effective to this end. A follow-up analysis helps identify actual sources of variations. Song, Mukherjee, and Zhang (2021) proposed a straightforward post-signal follow-up procedure in the bivariate Shewhart-type charts. We draw motivation from their article and present how the proposed MEWMA charts can be used for diagnosis analysis. If the scheme signals at the j^{th} test sample, we recommend the rules shown in Table 1 to determine the source of deterioration.

Table 1: Diagnosis Analysis after the scheme signals at the j^{th} stage.

	$E_{L,0,j} < H_L$	$E_{L,0,j} < H_L$	...	$E_{L,0,j} > H_L$	$E_{L,0,j} > H_L$	$E_{L,0,j} > H_L$	...
	$E_{L,1,j} < H_L$	$E_{L,1,j} < H_L$	...	$E_{L,1,j} < H_L$	$E_{L,1,j} < H_L$	$E_{L,1,j} < H_L$	...
	...	...	...	...	...	...	...
MEWMA-LC	$E_{L,k,j} > H_L$	$E_{L,k,j} > H_L$	...	$E_{L,k,j} < H_L$	$E_{L,k,j} > H_L$	$E_{L,k,j} > H_L$	...
	...	...	...	...	...	...	...
	$E_{L,r,j} < H_L$	$E_{L,r,j} > H_L$	...	$E_{L,r,j} < H_L$	$E_{L,r,j} < H_L$	$E_{L,r,j} > H_L$	...
	...	...	...	...	...	...	...
	$E_{C,0,j} < H_C$	$E_{C,0,j} < H_C$	...	$E_{C,0,j} > H_C$	$E_{C,0,j} > H_C$	$E_{C,0,j} > H_C$	...
	$E_{C,1,j} < H_C$	$E_{C,1,j} < H_C$	...	$E_{C,1,j} < H_C$	$E_{C,1,j} < H_C$	$E_{C,1,j} < H_C$	...
	...	...	...	...	...	...	...
MEWMA-CC	$E_{C,k,j} > H_C$	$E_{C,k,j} > H_C$	...	$E_{C,k,j} < H_C$	$E_{C,k,j} > H_C$	$E_{C,k,j} > H_C$	...
	...	...	...	...	...	...	...
	$E_{C,r,j} < H_C$	$E_{C,r,j} > H_C$	...	$E_{C,r,j} < H_C$	$E_{C,r,j} < H_C$	$E_{C,r,j} > H_C$	...
	...	...	...	...	...	...	...
Source of variations	a shift only in the k^{th}-variate	shifts in both the k^{th} and r^{th} variables	... ...	a shift only in the correlation	shifts in both the k^{th}-variate and correlation	shifts in the k^{th} and r^{th} variables and correlation	... ...

4 A review of competing schemes

The subsequent section presents a detailed performance comparison of our proposed EWMA schemes with four existing robust EWMA charts. Boone and Chakraborti (2012) proposed the Shewhart-type scheme based on the component-wise sign statistic. Chapter 9 of the book by Qiu (2014) extended it to the EWMA procedures, denoted as MEWMA-NS. As a competitor, we include this MEWMA-NS scheme. On the other hand, Mukherjee and Marozzi (2021) introduced a class of distribution-free charts based on specific distance

metrics for monitoring multivariate and high-dimensional processes. For a fair comparison, we construct three EWMA-Lepage schemes following the line of Mukherjee and Marozzi (2021), namely MEWMA-OR, MEWMA-IP and MEWMA-GM schemes. Next, we first introduce the designs of four competitive schemes in brief.

4.1 The MEWMA-NS scheme

The MEWMA-NS chart is EWMA-type and based on the multivariate forms of the sign, which is a simple and versatile nonparametric test. Suppose $\boldsymbol{\Psi_{jn}} = \left\{(X_{1ji'}, X_{2ji'}, \cdots, X_{dji'}),\ \ i' = 1, 2, \cdots, n\right\}$ be the j^{th} $(j = 1, 2, \ldots)$ test sample of size n, collected successively during the Phase-II monitoring. Let $\boldsymbol{\mu_0} = (\mu_{01}, \mu_{02}, \ldots, \mu_{0d})'$ be the $d-$dimensional location vector of the IC process distribution that is assumed known. For each of the d variables, we can define the componentwise sign statistic as follows:

$$\xi_{jk} = \sum_{i'=1}^{n} sgn\left(X_{kji'} - \mu_{0k}\right), \quad k = 1, 2, \ldots, d,$$

where $sgn(\cdot)$ is the sign function defined as

$$sgn\left(X_{kji'} - \mu_{0k}\right) = \begin{cases} 1 & \text{if} \quad X_{kji'} - \mu_{0k} > 0, \\ -1 & \text{if} \quad X_{kji'} - \mu_{0k} < 0. \end{cases}$$

It is well-known that ξ_{jk} is expected to be about 0 when the process is IC. If one or more components of test sample $\boldsymbol{\Psi_{jn}}$ have location shifts at the j^{th} monitoring stage, the corresponding components of $\boldsymbol{\xi_j} = (\xi_{j1}, \xi_{j2}, \ldots, \xi_{jd})'$ would deviate from 0. Therefore, the sign statistic can be used for monitoring shifts in the location parameters and the multivariate sign Shewhart charting statistic proposed by Boone and Chakraborti (2012) is

$$T_j^2 = \boldsymbol{\xi_j'}\hat{\mathbf{V}}_{\mathbf{j}}^{-\mathbf{1}}\boldsymbol{\xi_j},$$

where $\hat{\mathbf{V}}_{\mathbf{j}}$ denotes the estimator of the scale matrix of $\boldsymbol{\xi_j}$. The components $\hat{\nu}_{jl_1l_2}$ of $\hat{\mathbf{V}}_{\mathbf{j}}$, $l_1, l_2 = 1, 2, \ldots, d$ can be computed by

$$\hat{\nu}_{jl_1l_2} = \begin{cases} n & \text{if} \quad l_1 = l_2, \\ \sum_{i'=1}^{n} sgn\left(X_{l_1ji'} - \mu_{0l_1}\right) sgn\left(X_{l_2ji'} - \mu_{0l_2}\right) & \text{if} \quad l_1 \neq l_2. \end{cases}$$

Shewhart schemes efficiently detect large and isolated shifts but are ineffective in monitoring small and persistent shifts. Consequently, Qiu (2014) introduced the multivariate EWMA charting statistic as follows:

$$\mathbf{ENS_j} = \lambda\boldsymbol{\xi_j} + (1 - \lambda)\mathbf{ENS_{j-1}}, \quad \text{for} \quad j \geq 1,$$

where $\mathbf{E_0} = \mathbf{0}$, and $\lambda \in (0, 1]$ is a weighting parameter. Then, the MEWMA-NS scheme gives a signal of process mean shift if

$$\mathbf{ENS_j'}\boldsymbol{\Sigma}_{\mathbf{ENS_j}}^{-\mathbf{1}}\mathbf{ENS_j} > H_{NS},$$

where $\boldsymbol{\Sigma}_{\mathbf{ENS_j}}^{-\mathbf{1}} = \frac{2-\lambda}{\lambda}\hat{\mathbf{V}}_{\mathbf{j}}^{-\mathbf{1}}$, and H_{NS} is the UCL chosen to achieve a target MRL_0 value.

4.2 The MEWMA-OR scheme

Mukherjee and Marozzi (2021) proposed a class of Shewhart schemes using the Euclidean distance from the origin. In this subsection, we extend the Shewhart-type charts to the EWMA procedures. Suppose $(D_{01}, D_{02}, \ldots, D_{0m})$ be the Euclidean distances of the size m reference sample from the origin. Analogously, let $(D_{j1}, D_{j2}, \ldots, D_{jn})$ be the j^{th} test sample of size n of the Euclidean distances from origin (OR). Recall that the reference samples and test samples are independent, and therefore, $(D_{01}, D_{02}, \ldots, D_{0m})$ and $(D_{j1}, D_{j2}, \ldots, D_{jn})$ are also independent. Keep in mind that any process location or scale shifts is most likely indicated in the distribution of distance measures, see Jurečková and Kalina (2012) for more details. To this end, Mukherjee and Marozzi (2021) considered comparing reference samples and test samples using univariate two-sample linear rank tests based on the rankings of the pooled sample distance measures of $(D_{01}, D_{02}, \ldots, D_{0m})$ and $(D_{j1}, D_{j2}, \ldots, D_{jn})$. They constructed and evaluated three control charts using Wilcoxon, Ansari-Bradley and the Lepage statistics. Their studies showed that the monitoring scheme based on the Lepage statistic performed the best in most cases. Moreover, the Lepage control charts can be used to monitor the location and scale shifts jointly, and Marozzi (2009) showed that the Lepage test works well also for the general problem. Motivated by this, we only investigate the EWMA scheme based on the OR distance and Lepage statistic, denoted as the MEWMA-OR chart.

Revisit the Lepage statistic as shown in Equation (1) in subsection 2.1. Combining the reference distances and test distances and organizing all $N = m + n$ distance observations in ascending order, the rank of test distances $(D_{j1}, D_{j2}, \ldots, D_{jn})$ can be denoted as $R_{i'}, i' = 1, 2, \ldots, n$. The Lepage statistic is given by

$$L = \left(\frac{T_W - \mu_{T_W}}{\sigma_{T_W}}\right)^2 + \left(\frac{T_{AB} - \mu_{T_{AB}}}{\sigma_{T_{AB}}}\right)^2, \tag{5}$$

where

$$T_W = \sum_{i'=1}^{n} R_{i'}, \qquad T_{AB} = \sum_{i'=1}^{n} \left| \frac{N+1}{2} - R_{i'} \right|,$$

and μ_{T_*} and σ_{T_*} can be found in Song, Mukherjee, Marozzi, and Zhang(2020). The EWMA plotting statistic is designed by accruing the Lepage statistic sequentially as follows:

$$EOR_j = \lambda L_j + (1 - \lambda) EOR_{j-1},$$

where the starting value is set $EOR_0 = 2$. As mentioned in subsection 2.1, regardless of the shift's nature, the EWMA-Lepage statistic is anticipated to have a larger value when the process is OOC. Consequently, we only consider an UCL for the MEWMA-OR scheme in detecting any possible process changes.

4.3 The MEWMA-IP scheme

Commonly, the origin vector is remote from high-dimensional data clusters. To this end, Mukherjee and Marozzi (2021) suggested randomly selecting one reference sample to compute the interpoint (IP) distance metric rather than the origin and proposed a Shewhart-Lepage scheme. Analogously, we extend the Shewhart chart to the EWMA procedure, denoted as the MEWMA-IP scheme. Consider an arbitrary point $\mathbf{X_{0i_t}}$ of

the reference sample, where $1 \leq r \leq m$. Subsequently the IP distance can be computed by

$$D_{0i_s,i_t} = \|\mathbf{X_{0i_s}} - \mathbf{X_{0i_t}}\|, \quad s = 1, 2, \ldots, (m-1); \quad i_s \neq i_t,$$
$$D_{ji',i_t} = \|\mathbf{X_{ji'}} - \mathbf{X_{0i_t}}\|, \quad i' = 1, 2, \ldots, n; \quad j = 1, 2, \ldots.$$

It is easy to see that the distance vector $\left(D_{0i_1,i_t}, D_{0i_2,i_t}, \ldots, D_{0i_{m-1},i_t}\right)$ denotes the reference sample of size $m-1$ and $(D_{j1,i_t}, D_{j2,i_t}, \ldots, D_{jn,i_t})$ corresponds to the j^{th} test sample of size n. Note that, conditional independence of $m-1$ distance reference samples and n distance test samples at the j^{th} monitoring stage, one can compute the Lepage statistic L_j as in (6). Therefore, Mukherjee and Marozzi (2021) proposed a Shewhart-Lepage chart using IP reference and test distances. Then we design the corresponding EWMA-type charting statistic as follows:

$$EIP_j = \lambda L_j + (1-\lambda) EIP_{j-1}.$$

The process is deemed OOC if we see the monitoring statistic EIP_j for any j surpassing the associated UCL.

4.4 The MEWMA-GM scheme

Finally, Mukherjee and Marozzi (2021) argued that it is preferable to compute the distances of the reference and test samples using the spatial (geometric) median of the reference sample. The geometric median (GM) can minimise the total distances in Euclidean space to a discrete group of sample locations. The authors also noted that the GM distance-based scheme is nonparametric but not entirely distribution-free. Under the condition that the test sample size is not too small, this method is quite robust. Therefore, we also include the EWMA-Lepage scheme based on the GM distance as a competitor, abbreviated by the MEWMA-GM scheme.

Suppose $\mathbf{X_{0gm}}$ be the geometric median of the reference sample. Then the GM distances can be calculated by

$$D_{0i,0gm} = \|\mathbf{X_{0i}} - \mathbf{X_{0gm}}\|, \quad i = 1, 2, \ldots, m,$$
$$D_{ji',0gm} = \|\mathbf{X_{ji'}} - \mathbf{X_{0gm}}\|, \quad i' = 1, 2, \ldots, n; \quad j = 1, 2, \ldots.$$

Hereafter, we may define the distance vector $(D_{01,0gm}, D_{02,0gm}, \ldots, D_{0m,0gm})$ for the reference sample and for the test sample, $(D_{j1,0gm}, D_{j2,0gm}, \ldots, D_{jn,0gm})$. Then we can write the Lepage statistic L_j similar to that discussed in Equation (6) based on m GM distances of the reference sample and n GM distances of the j^{th} test sample. Then, the EWMA plotting statistic is given by

$$EGM_j = \lambda L_j + (1-\lambda) EGM_{j-1}.$$

The starting value $EGM_0 = 2$, and we only consider an UCL for the MEWMA-GM scheme in detecting any possible process changes.

5 Numerical results and performance comparisons

This section discusses the IC and OOC performance of the proposed monitoring schemes, say, the MEWMA-LC and MEWMA-CC. The statistical performance of the monitoring scheme is generally deeply investigated

in terms of some RL properties. The average run length (ARL) is popularly used to evaluate the performance of the schemes. However, the run-length distribution is likely to be right-skewed. It may be misleading to choose ARL as the performance evaluation indicator, which has been pointed out by several authors in recent ten years, like Khoo et al. (2012), Teoh et al. (2014), Hu, Castagliola, Tang and Zhong (2021), Mukherjee and Marozzi (2021). Therefore, we use the Median Run Length (MRL) instead of the ARL in this paper. The main advantage of MRL is its robustness, as the skewness of the run-length distribution has a lesser effect on it.

5.1 Determination of the control limits H_L and H_C.

To implement the proposed schemes, we need to determine the control limits achieving a pre-specified IC MRL, denoted as MRL_0. The nonlinear equation Median(RL(UCL))-MRL_0=0 for the UCL, such as H_L and H_C, is solved using Monte-Carlo simulation as the proposed charts are highly IC robust. One can also use bootstrapping in this regard. In this paper, we utilise the bisection method since this technique does not require derivatives of the underlying function. For each iteration of the bisection algorithm, we estimate the median using 10,000 independent runs, i.e., 10,000 times we run the control chart with simulated data until there is a signal.

A detailed guide for a practitioner on how to estimate the control limit could consist of the next steps:

Step 1: Choose two starting values A_1, A_2 in a way that Median(RL(A_1))-$\text{MRL}_0 < 0$ and Median(RL(A_2))-$\text{MRL}_0 > 0$;

Step 2: Check the sign of Median(RL($(A_1 + A_2)/2$))-MRL_0. If it is larger than 0, set $A_2 := (A_1 + A_2)/2$, otherwise set $A_1 := (A_1 + A_2)/2$;

Step 3: Keep performing step 2 till the absolute difference between the computed Median(RL($(A_1 + A_2)/2$)) and MRL_0 is less than or equal to 5. Then adopt $(A_1 + A_2)/2$ as the UCL;

5.2 IC performance

We need to determine the charting constants to implement the proposed procedures in advance. We utilise the R.4.0.5 software to calculate H_L and H_C based on the bisection algorithm described in subsection 5.1. One may simulate random samples from any continuous multivariate distribution, for example, generate both the reference sample and each test sample from a $d-$variate normal distribution. In this section, we present $d = 2$ and $d = 3$ for simplicity. The extension of the study for higher dimensions is straightforward. We consider the location parameters as $\boldsymbol{\mu_0} = \mathbf{0_d}$ and the scale matrix $\boldsymbol{\Sigma} = (\sigma_{0ij})$ as

$$\sigma_{0ij} = \begin{cases} \sigma_0^2 & \text{if} \quad i = j \\ \rho_{0ij}\sigma_{0i}\sigma_{0j} & \text{if} \quad i \neq j. \end{cases} \tag{6}$$

Here, we set $\sigma_{0i} = \sigma_{0j} = \sigma_0 = 1$ for all $i, j = 1, \ldots, d$ and $\rho_{0ij} = 0.5$, for all $i \neq j$. To investigate the IC performance, we select the reference sample size $m = 100, 150$, and the test sample size $n = 10, 15$. We set $\lambda = 0.05, 0.1, 0.15$ and 0.2 for the smoothing parameter. Finally, we choose the nominal MRL_0 as 250. We tabulate in Table 2 the computed UCL for the selected (m, n, λ) and target MRL_0. From Table 2, we observe that the UCL increases with λ when both m and n are fixed. Table 2 helps determine control

limits in some situations in practice. An R programme for computing the control limits is available from the authors upon request for different choices of charting parameters. Moreover, to assess the IC robustness of the proposed schemes, we consider some well-known continuous multivariate distributions, i.e. $d-$variate $t(3)$, Cauchy and exponential distributions. As expected, the obtained UCLs are also applicable for these non-normal distributions. That is, the attained MRL_0 is close to the target value of 250 in these situations. The details are shown and discussed in subsection 5.3.

Table 2: UCL values of the MEWMA-LC and MEWMA-CC schemes with some selected (m, n, λ) for the target $\text{MRL}_0 = 250$.

		$m = 100, n = 10$		$m = 100, n = 15$		$m = 150, n = 15$	
Dimension	λ	MEWMA-CC	MEWMA-LC	MEWMA-CC	MEWMA-LC	MEWMA-CC	MEWMA-LC
$d = 2$	0.05	1.5381	1.5481	1.5228	1.5232	1.5351	1.5452
	0.1	1.8503	1.8752	1.8491	1.8802	1.8451	1.8692
	0.15	2.1722	2.1631	2.1474	2.1821	2.1633	2.1691
	0.2	2.4482	2.4524	2.4255	2.4592	2.4383	2.4651
$d = 3$	0.05	1.6214	1.6256	1.6294	1.6394	1.6211	1.6391
	0.1	1.9892	1.9714	1.9681	2.0112	1.9721	1.9791
	0.15	2.2911	2.2993	2.2934	2.3251	2.2991	2.3282
	0.2	2.5793	2.6051	2.5792	2.5892	2.5992	2.6083

5.3 OOC performance comparisons

In this context, we compare the OOC performance of the above six multivariate EWMA schemes in terms of MRL. For the IC case, we consider the same parameter settings described in subsection 5.2. We select various combinations of (m, n, λ, d) values in the OOC simulation design. Specifically, m and n are set to 100 and 15, d is set to either 2 or 3, and λ is taken as four values 0.05, 0.1, 0.15 and 0.2. We also consider four representative distributions, namely d-variate normal (symmetric light-tailed), d-variate t with 3 d.f. (symmetric heavy-tailed), d-variate cauchy (symmetric very heavy-tailed) and d-variate exponential (skewed). Further, we consider the following shift settings when analyzing OOC performance. Define OOC location vector as $\boldsymbol{\mu_1} = \boldsymbol{\mu_0} + \boldsymbol{\theta}$, with each component in $\boldsymbol{\theta}$ being $\theta_p = \mu_{1p} - \mu_{0p}$, $p = 1, 2, \ldots, d$. Recall that we set $\boldsymbol{\mu_0} = \mathbf{0_d}$, then the OOC location vector is

$$\boldsymbol{\mu_1} = \boldsymbol{\theta}.$$

On the other side, the OOC scale matrix $\boldsymbol{\Sigma_1} = (\sigma_{1ij})$ is stated as

$$\sigma_{1ij} = \begin{cases} \sigma_{1p}^2 & \text{if} \quad i = j = p, \quad p = 1, 2, \ldots, d. \\ \rho_{1ij}\sigma_{1i}\sigma_{1j} & \text{if} \quad i \neq j, \quad i, j = 1, 2, \ldots, d. \end{cases}$$

We examine the effectiveness of the six schemes by taking into account the shifts following four different kinds in the location vector, scale matrix or both:

i. **Shifts only in location vector, denoted as "LS"**, is acquired by examining the following two different location shift situations, keeping the IC scale matrix invariant:

LS1. We change only the first component μ_{01} of the IC location vector from 0 to $\mu_{11} = \theta_1$, where θ_1 is set to $0.1, 0.2, 0.3, 0.4, 0.5, 0.6, 0.7, 0.8, 0.9, 1, 1.2, 1.4, 1.6, 1.8$ and 2.

LS2. We consider only two elements of the IC location vector shifting simultaneously, i.e., we change μ_{01} to $\mu_{11} = \theta_1$, as described in the LS1 scenario, whilst shifting the second element μ_{02} of the IC location vector from 0 to $\mu_{12} = \theta_2 = 0.5$.

ii. Shifts only in the diagonals of the scale matrix, referred to as "DS", is achieved by shifting the diagonal components of the IC scale matrix from σ_0^2 to $\sigma_{1p}^2 = \delta_p$, where δ_p is the shift size, with the off-diagonal components are left unchanged. To be specific, we consider two cases as follows:

DS1. The DS1 case is only the first element of the diagonal has a shift of size δ_1, where $\delta_1 = 1.1, 1.2, 1.3, 1.4, 1.5, 1.6, 1.7, 1.8, 1.9, 2$.

DS2. The DS2 case is changing the first component of the diagonal to δ_1; meanwhile, the second element of the diagonal shifts to the fixed value $\delta_2 = 1.5$. That is, the DS1 case considers only one component changing, whereas the second investigates two components shifting simultaneously.

iii. Shifts only in the off-diagonals of the scale matrix, called "OD", is obtained by changing only the $(1, 2)$ off-diagonal element ρ_{012} of the IC scale matrix from 0.5 to ρ_{112}, where ρ_{112} takes the values of $0.1, 0.2, 0.3, 0.4, 0.5, 0.6, 0.7, 0.8, 0.9$.

iv. Mixed shifts in both location vector and scale matrix, named "MS", stands for simultaneous location and scale matrix shifts. For a comprehensive assessment, we consider three diverse shift circumstances as follows:

MS1. In MS1 case, we keep μ_{01} shift from 0 to 0.5. In the meantime, we change the first element of the diagonal from 1 to δ_1, where δ_1 is taken as $1.1, 1.2, 1.3, 1.4, 1.5, 1.6, 1.7, 1.8, 1.9$ and 2. In contrast, the other IC elements are invariant.

MS2. In MS2 case, we change the first element of the diagonal from 1 to 1.5. We change the first component μ_{01} of the IC location vector from 0 to $\mu_{11} = \theta_1$, where θ_1 is selected to $0.1, 0.2, 0.3, 0.4, 0.5, 0.6, 0.7, 0.8, 0.9$ and 1. Apart from that, the other components are IC.

MS3. We change μ_{01} in MS3 case from 0 to 0.5 and the first diagonal element from 1 to 1.5. At the same time, the $(1, 2)$ off-diagonal element ρ_{012} of the IC scale matrix shifts from 0.5 to ρ_{112}, where ρ_{112} is chosen to $0.1, 0.2, 0.3, 0.4, 0.5, 0.6, 0.7, 0.8$ and 0.9.

The results of the above shift scenarios for $d = 2$ and $d = 3$ are given in Figures 1-14. We also conducted simulations with various shift types, and the results show that the general conclusions below are valid. For conciseness, we omit the details for the other combinations.

From Figures 1-8, in the case of the d-variate ($d = 2, 3$) Normal processes, we see the following results:

i The MEWMA-NS scheme is the best in detecting a pure small location change in only one of the variables, say LS1 shift, but the proposed MEWMA-LC and MEWMA-CC schemes remain very competitive. It is expected as the MEWMA-NS scheme is designed mainly for monitoring location parameters of multivariate processes. When there are shifts in two location parameters, our proposed EWMA schemes perform almost the same as the MEWMA-NS scheme, especially with small λ. It is noteworthy that the median of the process is assumed known when using the MEWMA-NS scheme. In addition, the MEWMA-NS chart is not distribution-free for small samples, and the scale matrix of the multivariate component-wise sign statistic may be singular in some cases.

ii The MEWMA-CC scheme is outstanding for DS1 shift, i.e., one of the variables has a pure scale shift. The MEWMA-LC scheme also gives better results. These findings are valid irrespective of the value of λ and more obvious when $d = 3$. For simultaneous scale shifts in two variables (DS2), the MEWMA-GM scheme performs slightly better than the other schemes in most situations. The proposed MEWMA-CC scheme offers better performance for small scale shift ($\theta_1 = 1.1, 1.2$) with large λ, $\lambda = 0.15, 0.2$. It is worth noting that the MEWMA-NS scheme shows severe MRL bias ($\text{MRL}_1 > \text{MRL}_0$).

iii In the case of OD shift, when there is a downward shift in off-diagonal of the scale matrix ($\rho_{112} < 0.5$), the proposed MEWMA-LC and MEWMA-CC schemes offer the best performance, while the other charts show severe MRL bias. For upward shifts ($\rho_{112} > 0.5$), all considered schemes perform similarly except that the MEWMA-NS scheme has MRL bias. The MEWMA-OR and MEWMA-IP schemes perform the best for small upward shifts in off-diagonal of the scale matrix. However, for a moderate to large shift, the MEWMA-LC stands for the best scheme, especially with small λ.

iv For the three cases of MS shift, the proposed MEWMA-LC and MEWMA-CC schemes offer the best performance in all considered scenarios. The MEWMA-NS scheme also gives a competitive performance in most cases.

The OOC performance of six competing schemes for three multivariate non-normal processes is presented in Figures A1-A6 in the Appendix. To save space, we only present the results of $\lambda = 0.1$. The results for other choices of λ are comparable to the general conclusions given below.

i The numerical results of comparison with d-variate $t(3)$ distribution are similar to the case under multivariate Normal distribution. However, the MRL_1 value corresponding to each shift case under $t(3)$ distribution is larger than that under the Normal distribution. This finding indicates that all considered schemes have better detection ability under Normal distribution than $t(3)$ distribution.

ii The comparison outcomes under the d-variate Cauchy distribution are analogous to those under the multivariate Normal and $t(3)$ distributions. Moreover, compared with $t(3)$ distribution, all charts' capability in monitoring Cauchy processes is less as the corresponding MRL_1 increases. We also observe that our proposed two schemes outperform other charts in detecting mixed shifts for Normal and $t(3)$ distributions. In contrast, the MEWMA-NS scheme performs slightly better than the proposed MEWMA-LC and MEWMA-CC charts for Cauchy distribution.

iii When the distribution is d-variate exponential, the conclusions for LS, DS and OD shifts are close to those under Normal and $t(3)$ distributions, except for the following two points: (i) The inspection efficiency of all considered charts are significantly improved in detecting pure location shifts (LS2); (ii) The performance of the MEWMA-OR scheme under Cauchy distribution is enhanced compared with its previous results under other distributions. Under exponential distribution, the proposed two charts and the MEWMA-NS chart perform much better than the other charts in monitoring mixed shift.

The OOC performance of different EWMA monitoring schemes may not be comparable with the same weighting parameter λ, as pointed out in Qiu (2018). Therefore, we further compare their optimal OOC performance to make a fair comparison. That is, we select the weighting parameter of each chart by

minimizing the MRL_1 value for detecting a given shift. All other settings are similar to those in the previous comparison. We present the calculated minimum MRL_1 of the six schemes for d-variate Normal distribution in Figures 9 and 10. The figures show that similar conclusions to those in the previous comparison can be made here regarding the optimal performance of the six schemes. For the other non-normal distribution, the results are also similar. The details are omitted here to save space.

Overall, we can conclude that our proposed EWMA procedures are always the best available scheme or the nearest rival of the best available scheme, especially for scale shifts. Apart from that, it is worth mentioning that our proposed procedures can identify which of the variables is the source of assignable causes or the dependence structure is responsible for the signal. Next, we discuss the implementation strategies of the above six procedures with real data.

6 Real data applications

This section exhibits a real data study to illustrate the practical applications of the proposed charts and the comparison among the six competitive schemes as described in the previous section. Next, we consider the joint monitoring of the lengths and diameters of cork stoppers from the manufacturing industry.

The length and diameter are two essential physical characteristics of cork stoppers that are required to monitor simultaneously. Also, it is essential to identify if the shift happened in length, diameter, or both in case an OOC signal is produced. We illustrate the six EWMA schemes using the available data obtained from a manufacturing unit. Figueiredo and Gomes (2013) and Li, Mukherjee, Su, and Xie (2016) monitored the same in other contexts where component-wise assessment issues were not considered. We first focus on establishing a Phase-I sample. To this end, 180 pairs of observations on corks' lengths and diameters are collected. We employ various methods of distribution-free Phase-I analysis using different codes available in the R package *dfphase1*: Interested readers may see Capizzi and Masarotto (2018) for more details. The results show that there is no OOC signal. Therefore, these 180 pairs of observations may safely be taken as Phase-I samples. That is, the reference sample size is $m = 180$.

Next, we proceed to Phase-II monitoring. We consider 34 subgroups of size $n = 10$ as the Phase-II data (test data). We present the reference data and test data in Figure 11. Finally, based on Section 3, we illustrate the implementation of the proposed schemes for 34 subgroups of size $n = 10$ to monitor the lengths and diameters of cork stoppers. We conduct a simulation study, as in Section 5.1, to compute the UCLs H_L and H_C of the MEWMA-LC and MEWMA-CC charts, respectively, for $m = 180, n = 10, \lambda = 0.1$ and a target $\text{MRL}_0 = 250$. For the other four competitive schemes, we also employ Monte-Carlo simulation to calculate UCLs to achieve $\text{MRL}_0 = 250$. We enumerate the values of UCL for each scheme in Table 3. In the same table, we tabulate 34 plotting statistics for each chart and indicate the test samples that trigger an OOC signal in bold. It is interesting to note that some values of the plotting statistics are infinity (∞) in Table 3, resulting from at least one of the estimated p-values corresponding to the components of the proposed charts being zero. A p-value of zero indicates that the relevant Lepage or Cucconi statistic is very large, which is strong evidence of process OOC signal. Subsequently, we display the observed values of 34 plotting statistics for the six schemes in Figure 12.

One needs to address the post-signal follow-up procedure in implementing a joint monitoring scheme using a single plotting statistic. It is worth noting that only our proposed charts can additionally indicate which variable has the problem. We carry out a diagnostic check following the guidelines of Table 1. To this end,

we calculate the coordinates $(E_{L,0,j}, E_{L,1,j}, E_{L,2,j})$ for the MEWMA-LC scheme and $(E_{C,0,j}, E_{C,1,j}, E_{C,2,j})$ for the MEWMA-CC scheme, $j = 1, 2, \ldots, 34$, which can be obtained following the implementation steps outlined in Section 3. Note that the coordinates represent a sample's length, diameter and scale components to identify which of the two variables is responsible for the shift or whether the dependence structure is responsible for the signal. We tabulate the three component values in Table 3. We use the bold to indicate which component(s) is (are) the cause of deterioration.

Table 3 and Figure 12 both display that the proposed schemes show signals from the 16^{th} test sample onwards, which strongly indicates a shift in the process. The MEWMA-NS chart gives the first signal at test sample 25. Overall, seven out of 34 subgroups are providing OOC signals. The MEWMA-IP chart offers the signals from test sample 16 to sample 21. Test samples from 22 until 32 return to the IC state, but the values for the 33^{th} and 34^{th} samples exceed the corresponding UCL again. Based on the MEWMA-OR scheme, only the values of the plotting statistics for the last three test samples are above UCL. The MEWMA-GM scheme shows a signal quickly at the 11^{th} test sample, and the values for test samples 12 to 22 fall marginally above or below the UCL. Finally, test samples 32 to 34 indicate strong OOC signals.

Following the signals, diagnosing the sources of assignable causes is interesting. Based on the MEWMA-LC scheme, we observe that from test sample 16 until sample 34, the values of both the length and scale components exceed the H_L. Still, the diameter component values are larger than the H_L from the 23^{th} test sample onwards: Thus, we can conclude that there is evidence of a shift in the length and scale components for test samples 16 to 34. Whereas, for the 23^{rd} to 34^{th} test samples, all three components are the source of variations. On the other hand, we observe from the diagnostic results for the MEWMA-CC chart that the values of the scale component from test sample 16 to sample 34 are above the H_C. The values of the length component for test samples 16, 17, 18 and 34 exceed the H_C. Moreover, the diameter component values are larger than the H_C from the 24^{th} test sample onwards: Therefore, the MEWMA-CC scheme shows that the possible assignable cause of test samples 16 to 18 is both length and scale components. The diagnosis analysis for the 19^{th} to 23^{rd} test samples indicates a possibility of shift only in the scale element. Further, there is evidence of a shift in the diameter and scale components from test sample 24 to sample 33, and the possible assignable cause of test sample 34 is all three components.

7 Concluding Remarks

In this paper, we develop two robust EWMA-type procedures for monitoring multivariate processes, referred to as the MEWMA-LC and MEWMA-CC schemes. The newly designed plans can monitor the location-scale of the components in tandem, say, the marginal distributions and the copula. The copula describes the dependence structure between the variables. We present the implementation steps and investigate the IC and OOC performance of the proposed schemes. A performance comparison of our proposed schemes is made with four existing nonparametric schemes under four representative multivariate models by an extensive simulation study. The overall performance of the MEWMA-CC scheme is found attractive for a class of shifts, especially for monitoring scale shifts. Moreover, unlike many existing schemes, the two proposed schemes offer excellent post-signal follow-up procedures that can classify the signal source, whether the shift occurs in the variable(s) or the dependence structure.

We illustrate six EWMA schemes using a real dataset, which is monitoring bivariate processes involving the lengths and diameters of cork stoppers. We may conclude that our proposed schemes are pretty helpful in

practice. Designing CUSUM charts using the plotting statistics developed in this article will be interesting. More research in this direction is required for the dependent sequence of observations. We leave this for future research.

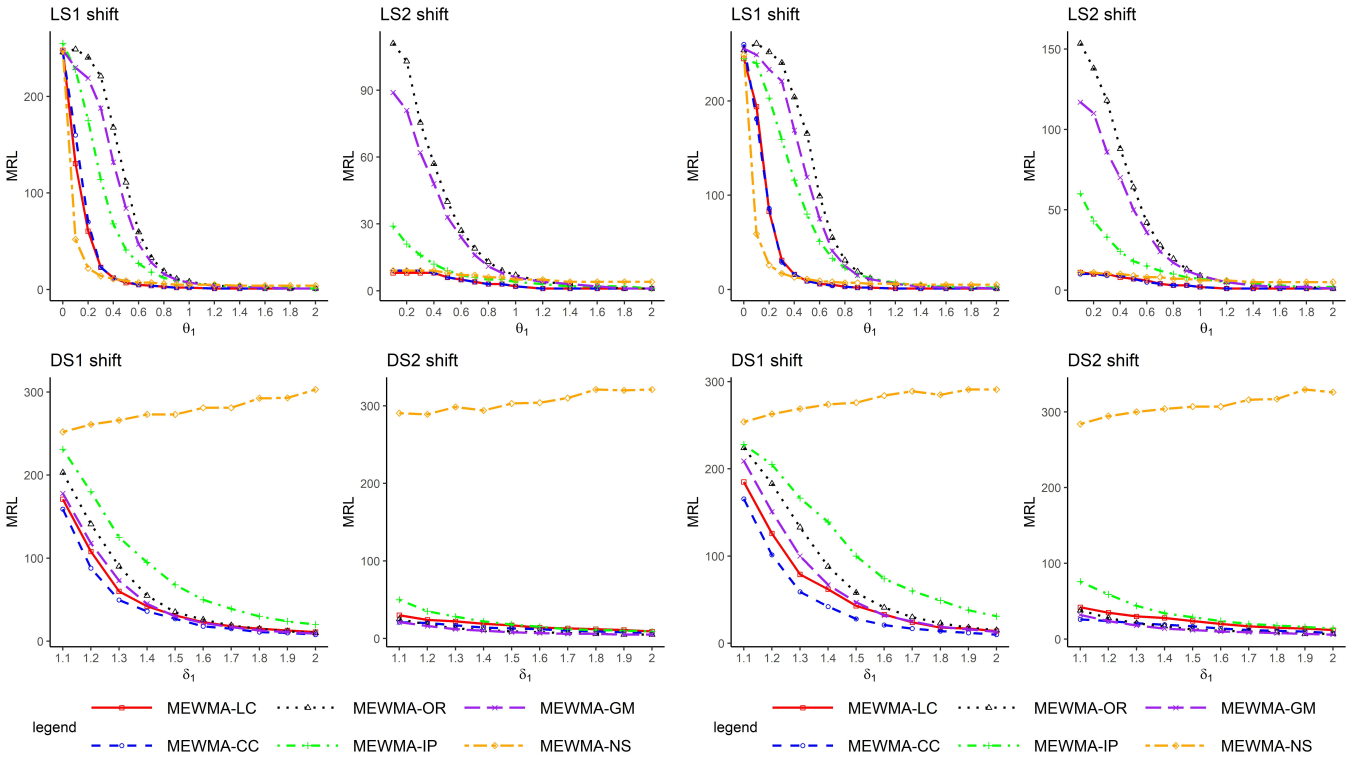

(a) $d = 2$ (b) $d = 3$

Figure 1: OOC performance comparisons of six multivariate EWMA schemes under d-variate **Normal** distribution for **LS and DS shifts** with $m = 100, n = 15, \boldsymbol{\lambda = 0.05}$ and the target $\text{MRL}_0 = 250$. Note that the figures in the first and second columns are for $d = 2$ and the figures in the third and fourth columns are for $d = 3$. The first row is OOC performance under shift situation-LS and the second row is OOC performance under shift situation-DS.

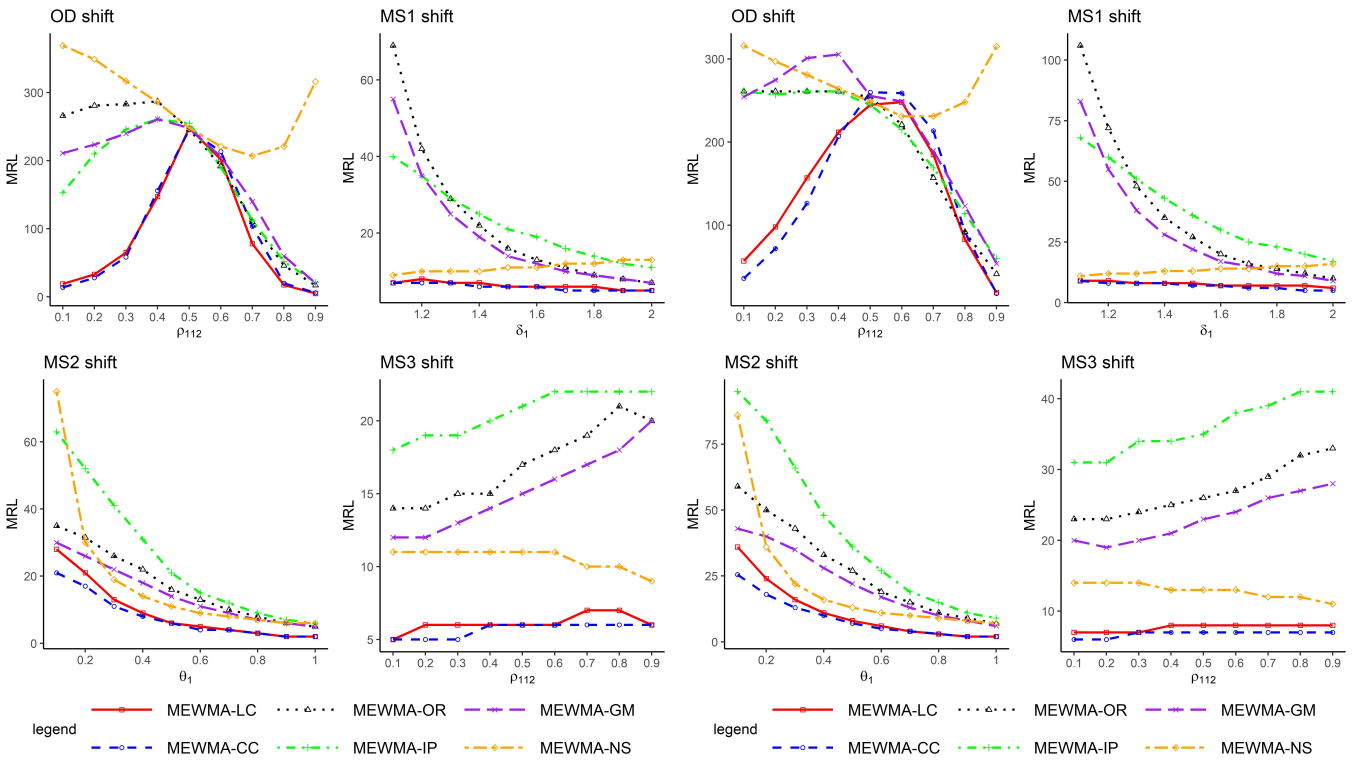

(a) $d = 2$ (b) $d = 3$

Figure 2: OOC performance comparisons of six multivariate EWMA schemes under d-variate **Normal** distribution for **OD and MS shifts** with $m = 100, n = 15, \boldsymbol{\lambda = 0.05}$ and the target $\text{MRL}_0 = 250$. Note that the figures in the first and second columns are for $d = 2$ and the figures in the third and fourth columns are for $d = 3$. The first figure in the first row is OOC performance under shift situation-OD and the others are OOC performance under shift situation-MS.

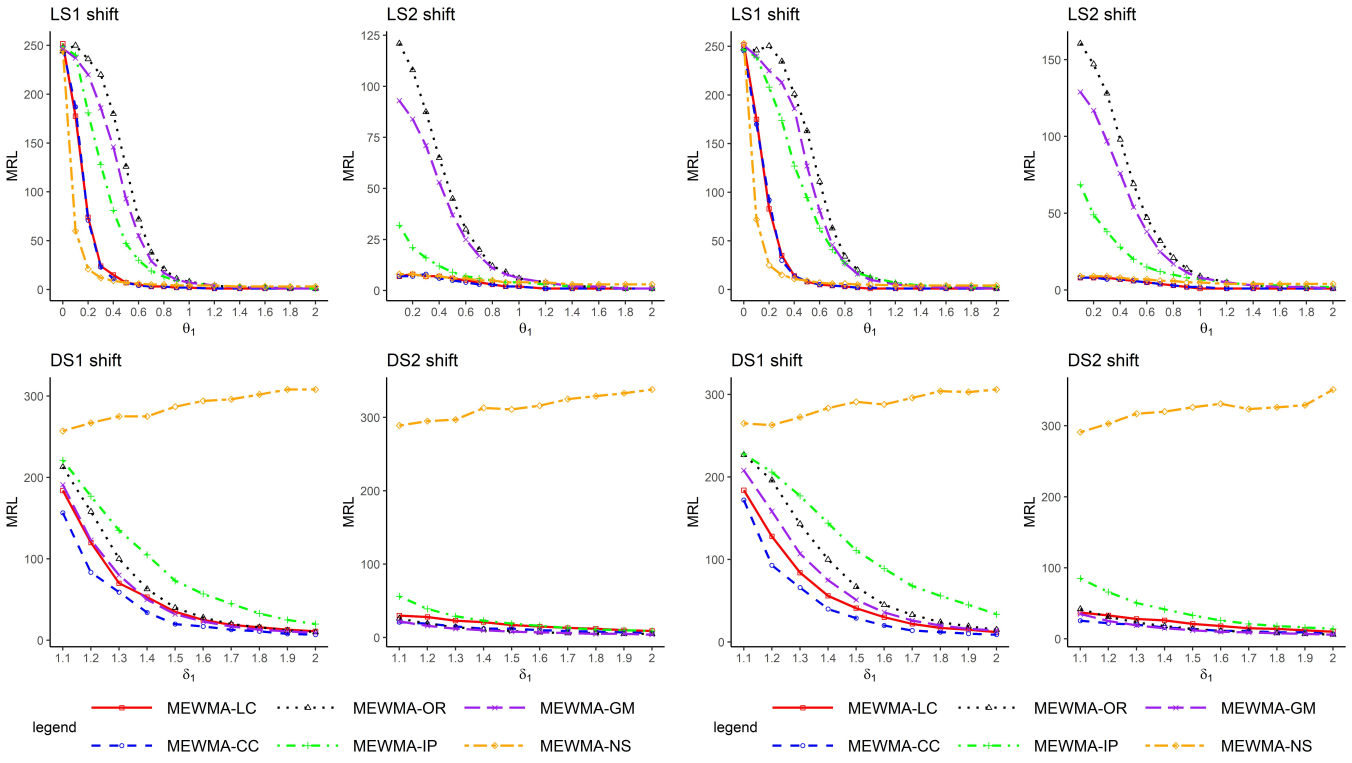

(a) $d = 2$ (b) $d = 3$

Figure 3: OOC performance comparisons of six multivariate EWMA schemes under d-variate **Normal** distribution for **LS and DS shifts** with $m = 100, n = 15, \boldsymbol{\lambda = 0.1}$ and the target $\text{MRL}_0 = 250$. Note that the figures in the first and second columns are for $d = 2$ and the figures in the third and fourth columns are for $d = 3$. The first row is OOC performance under shift situation-LS and the second row is OOC performance under shift situation-DS.

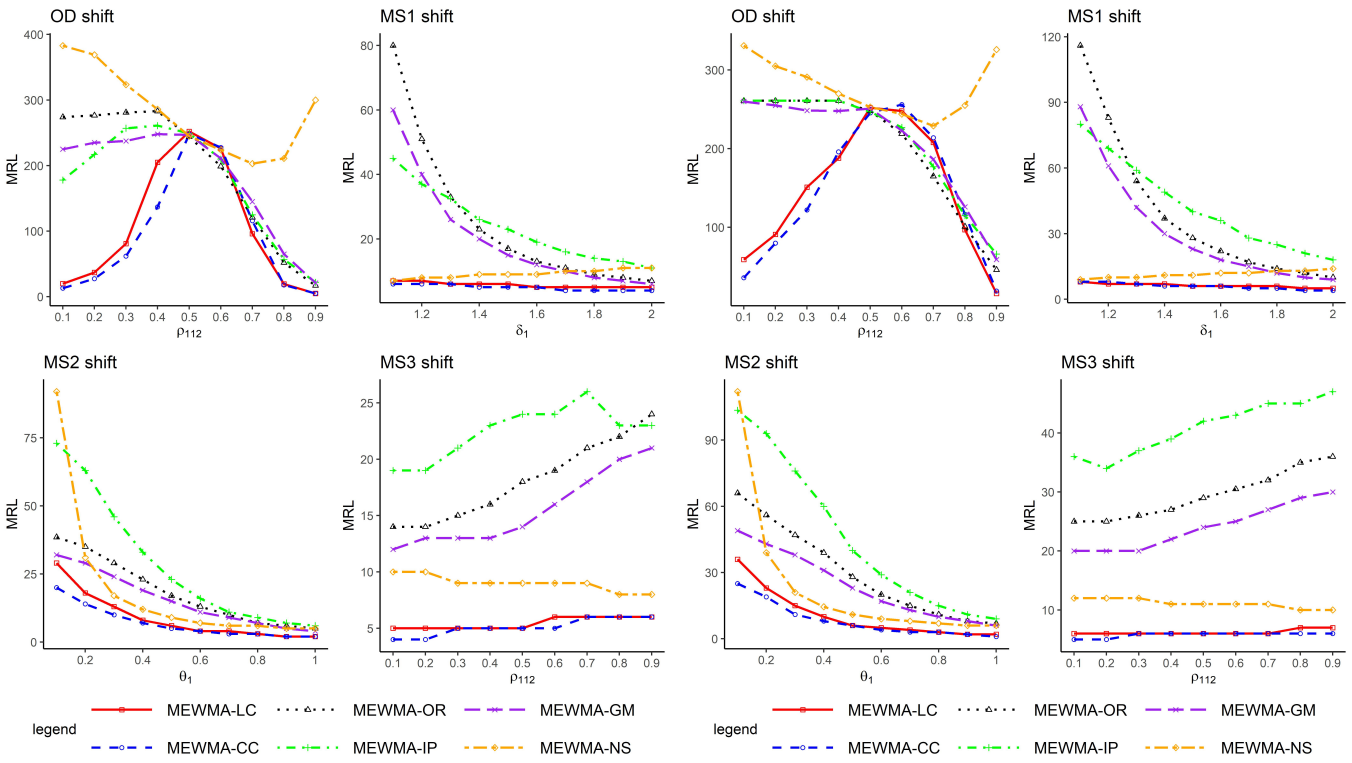

(a) $d = 2$ (b) $d = 3$

Figure 4: OOC performance comparisons of six multivariate EWMA schemes under d-variate **Normal** distribution for **OD and MS shifts** with $m = 100, n = 15, \boldsymbol{\lambda = 0.1}$ and the target $\text{MRL}_0 = 250$. Note that the figures in the first and second columns are for $d = 2$ and the figures in the third and fourth columns are for $d = 3$. The first figure in the first row is OOC performance under shift situation-OD and the others are OOC performance under shift situation-MS.

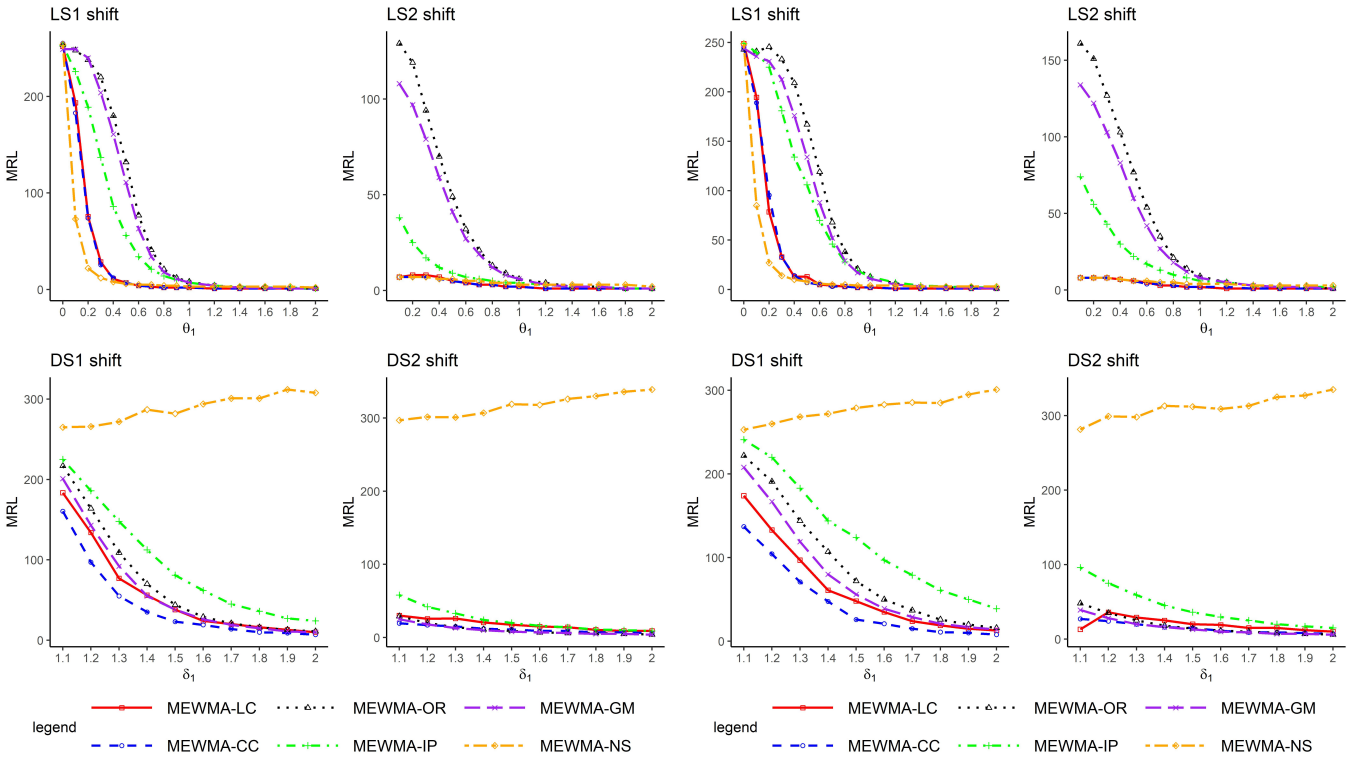

(a) $d = 2$ (b) $d = 3$

Figure 5: OOC performance comparisons of six multivariate EWMA schemes under d-variate **Normal** distribution for **LS and DS shifts** with $m = 100, n = 15, \boldsymbol{\lambda = 0.15}$ and the target $\text{MRL}_0 = 250$. Note that the figures in the first and second columns are for $d = 2$ and the figures in the third and fourth columns are for $d = 3$. The first row is OOC performance under shift situation-LS and the second row is OOC performance under shift situation-DS.

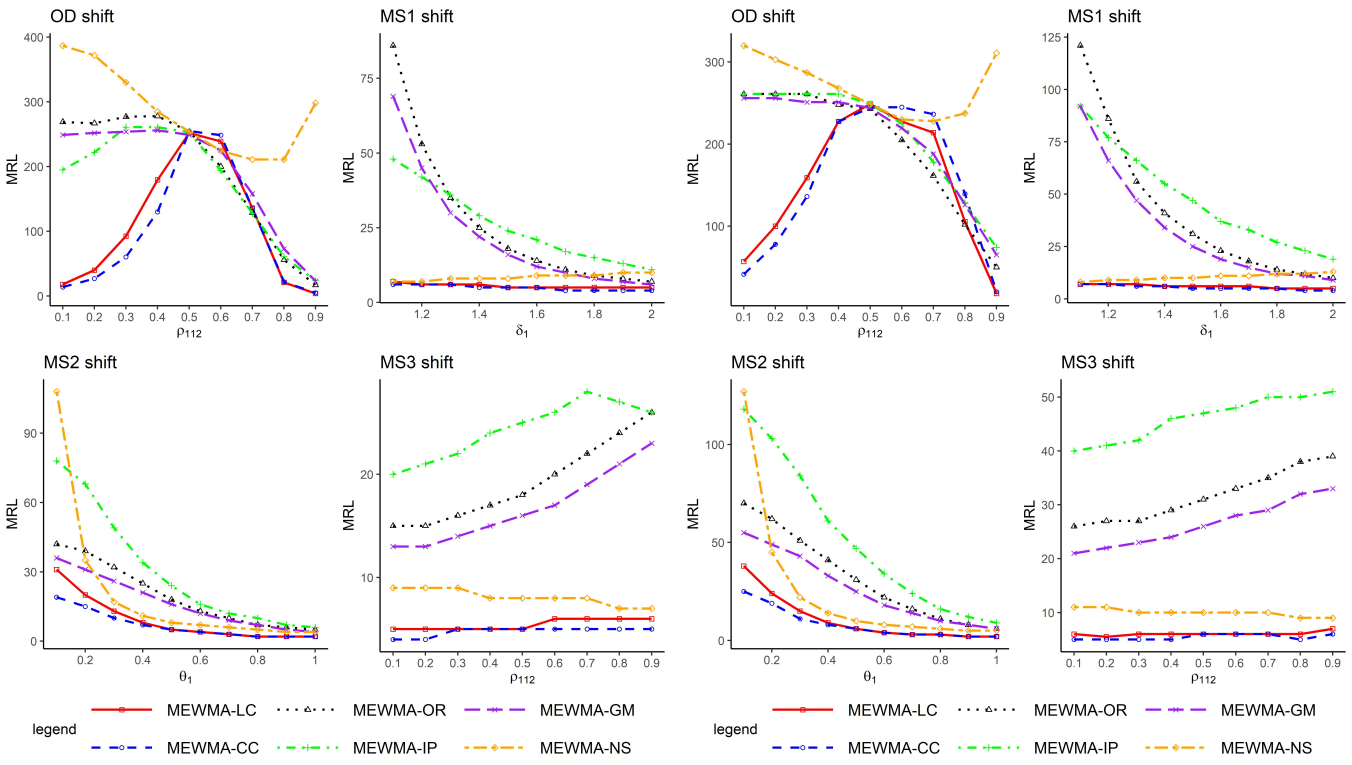

(a) $d = 2$ (b) $d = 3$

Figure 6: OOC performance comparisons of six multivariate EWMA schemes under d-variate **Normal** distribution for **OD and MS shifts** with $m = 100, n = 15, \boldsymbol{\lambda = 0.15}$ and the target $\text{MRL}_0 = 250$. Note that the figures in the first and second columns are for $d = 2$ and the figures in the third and fourth columns are for $d = 3$. The first figure in the first row is OOC performance under shift situation-OD and the others are OOC performance under shift situation-MS.

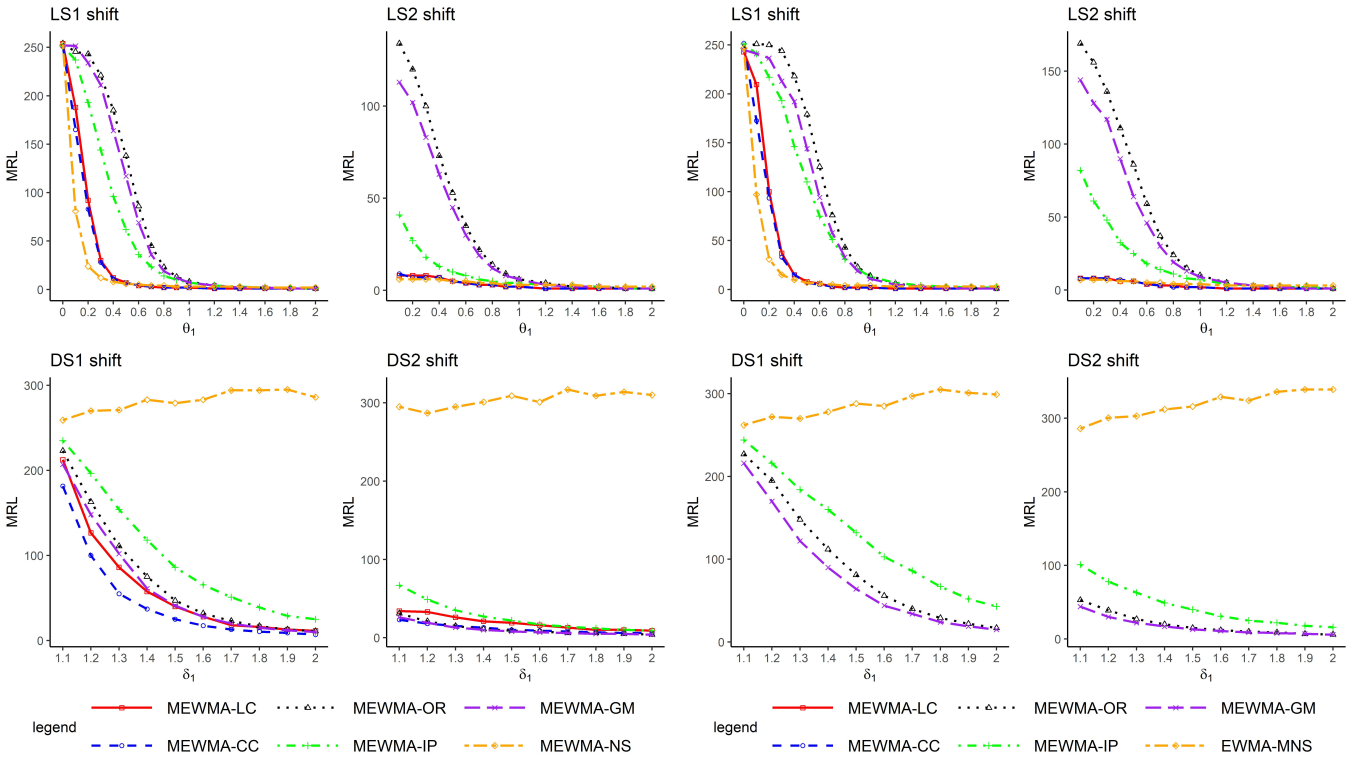

(a) $d = 2$ (b) $d = 3$

Figure 7: OOC performance comparisons of six multivariate EWMA schemes under d-variate **Normal** distribution for **LS and DS shifts** with $m = 100, n = 15, \boldsymbol{\lambda = 0.2}$ and the target $\text{MRL}_0 = 250$. Note that the figures in the first and second columns are for $d = 2$ and the figures in the third and fourth columns are for $d = 3$. The first row is OOC performance under shift situation-LS and the second row is OOC performance under shift situation-DS.

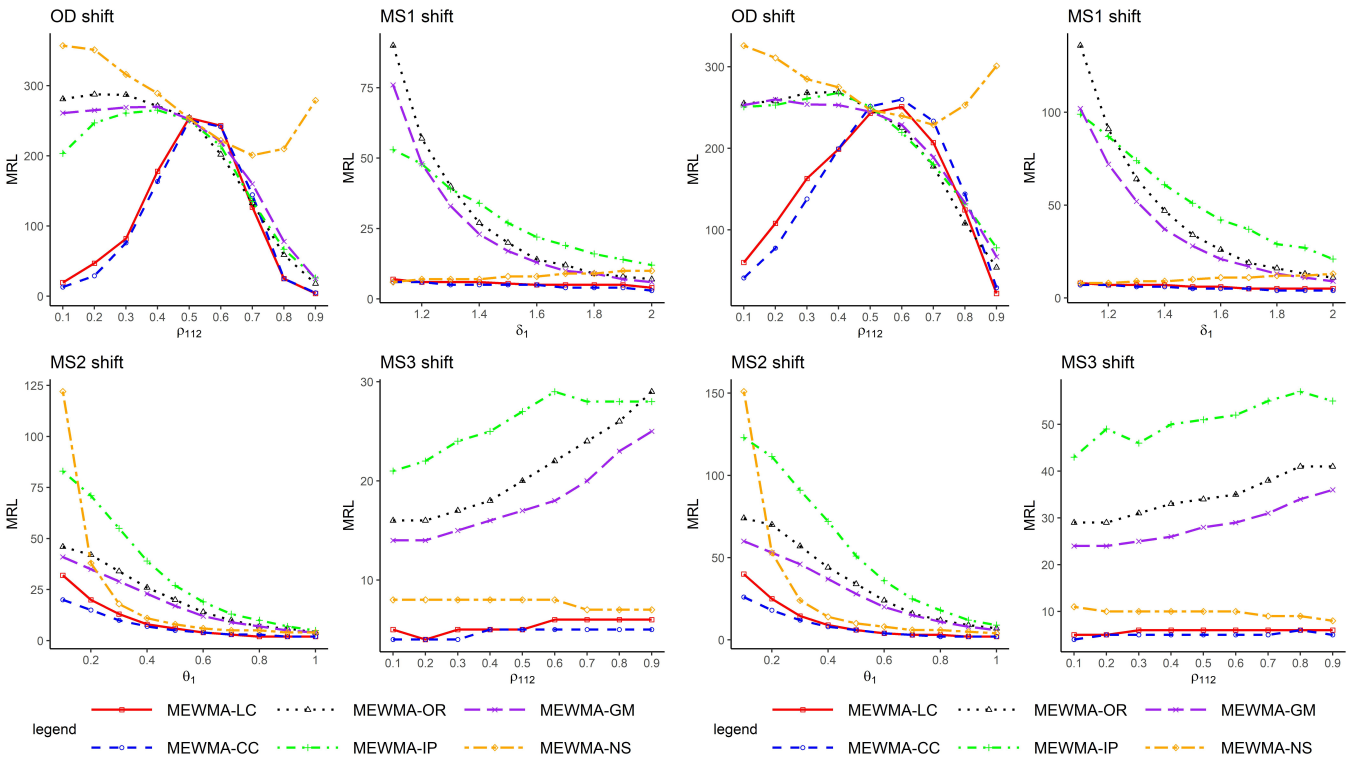

(a) $d = 2$ (b) $d = 3$

Figure 8: OOC performance comparisons of six multivariate EWMA schemes under d-variate **Normal** distribution for **OD and MS shifts** with $m = 100, n = 15, \boldsymbol{\lambda = 0.2}$ and the target $\text{MRL}_0 = 250$. Note that the figures in the first and second columns are for $d = 2$ and the figures in the third and fourth columns are for $d = 3$. The first figure in the first row is OOC performance under shift situation-OD and the others are OOC performance under shift situation-MS.

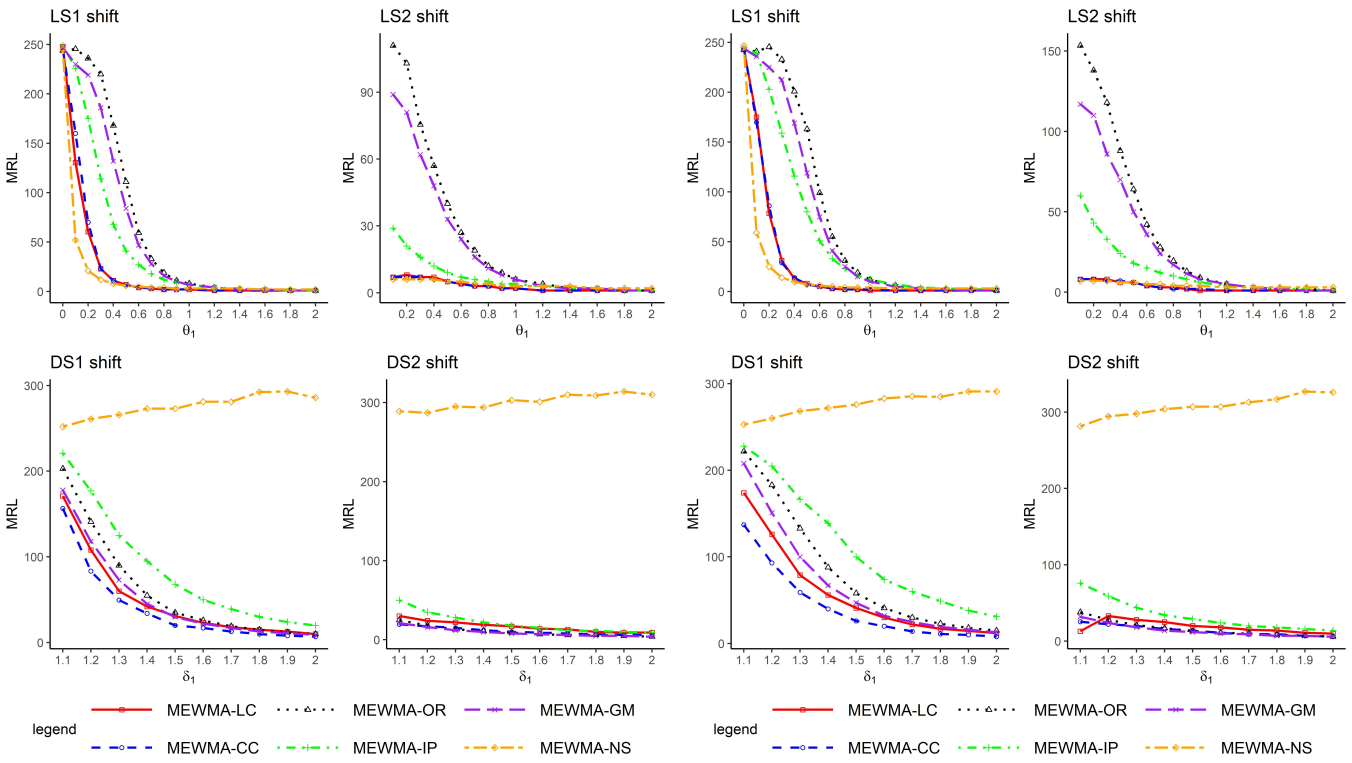

(a) $d = 2$ (b) $d = 3$

Figure 9: Computed **optimal** MRL_1 values of six multivariate EWMA schemes under d-variate **Normal** distribution for **LS and DS shifts** with $m = 100, n = 15$ and the target $\text{MRL}_0 = 250$. Note that the figures in the first and second columns are for $d = 2$ and the figures in the third and fourth columns are for $d = 3$. The first row is OOC performance under shift situation-LS and the second row is OOC performance under shift situation-DS.

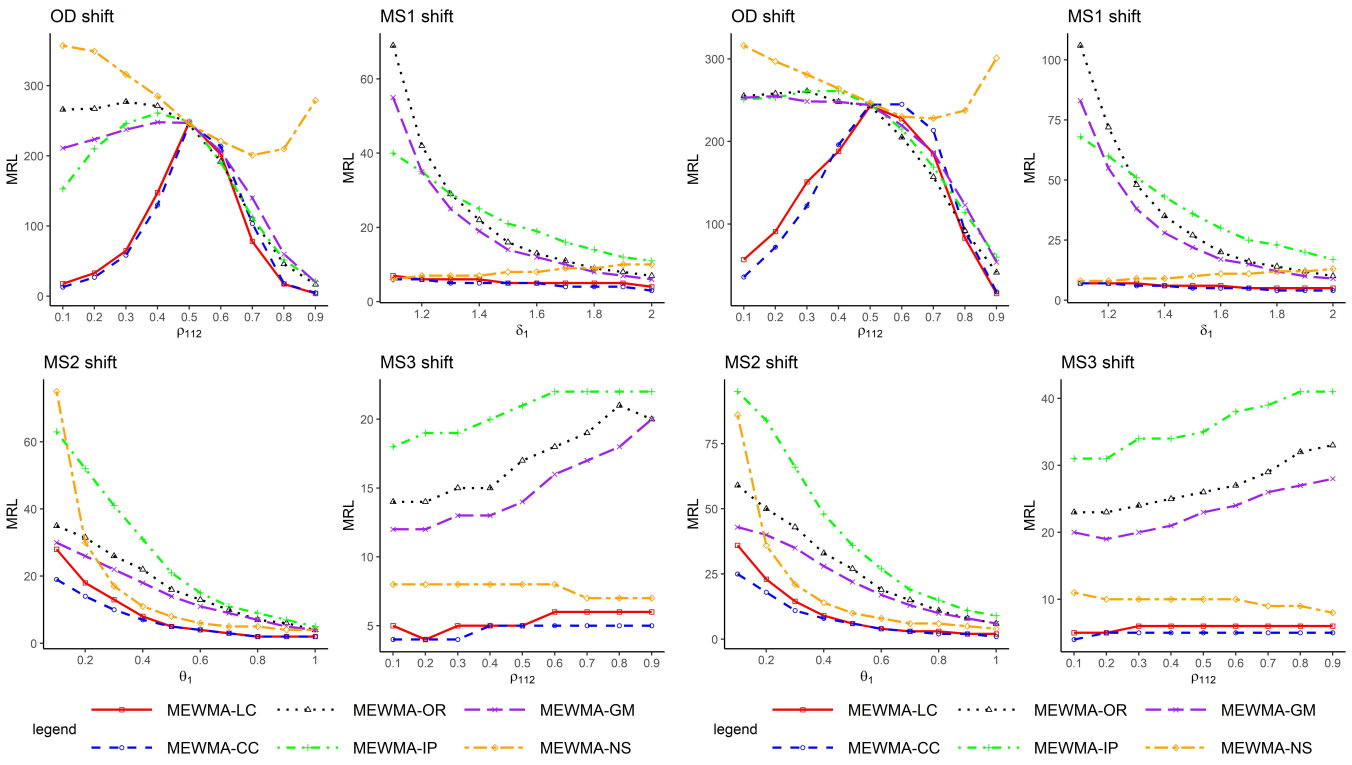

(a) $d = 2$ (b) $d = 3$

Figure 10: Computed **optimal** MRL_1 values of six multivariate EWMA schemes under d-variate **Normal** distribution for **OD and MS shifts** with $m = 100, n = 15$ and the target $\text{MRL}_0 = 250$. Note that the figures in the first and second columns are for $d = 2$ and the figures in the third and fourth columns are for $d = 3$. The first figure in the first row is OOC performance under shift situation-OD and the others are OOC performance under shift situation-MS.

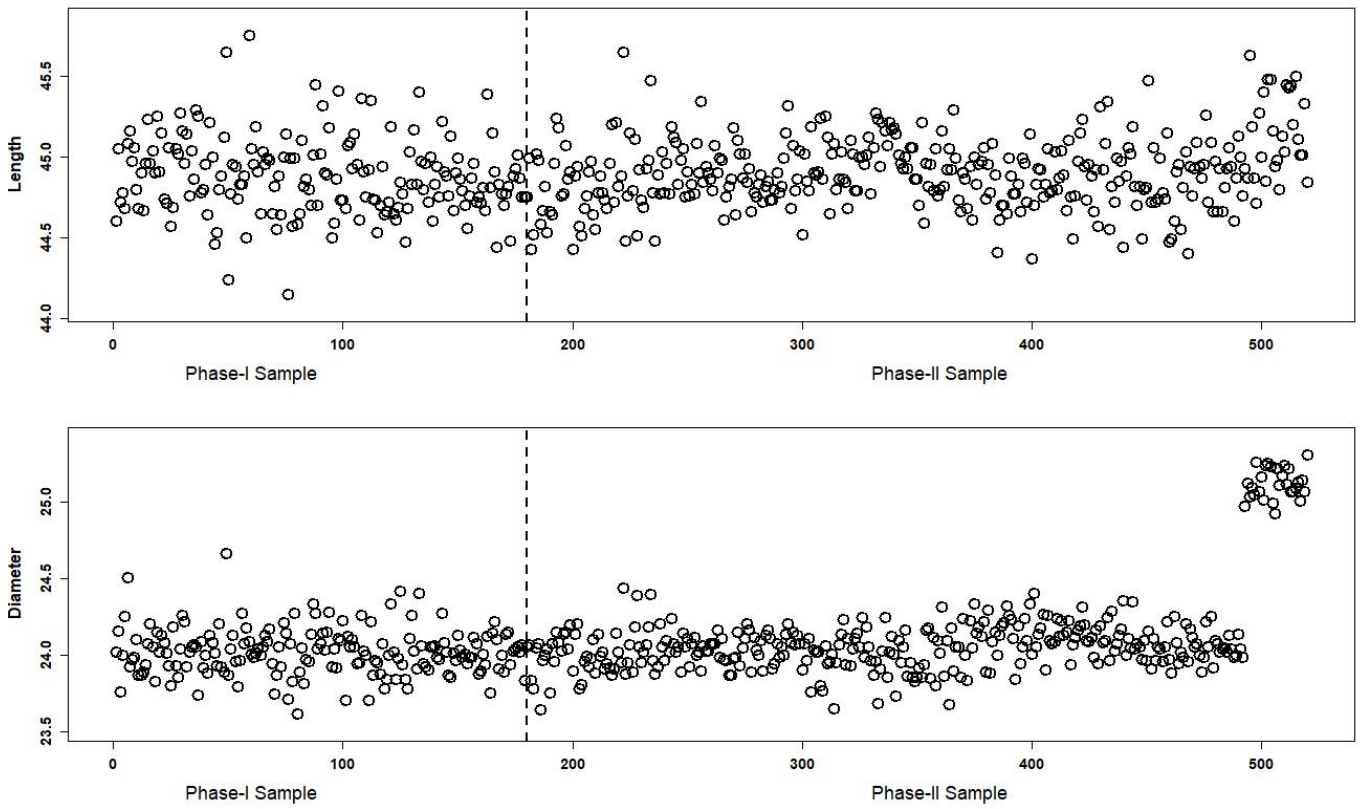

Figure 11: The Phase-I and Phase-II data on corks' lengths and diameters.

Table 3: Plotting statistics and component-wise assessment for lengths and diameters of cork stoppers.

Sample No	MEWMA-LC $UCL = 1.8851$				MEWMA-CC $UCL = 1.8706$				MEWMA-NS $UCL = 22.1$	MEWMA-OR $UCL = 3.259$	MEWMA-IP $UCL = 3.249$	MEWMA-GM $UCL = 3.256$
	Statistics	Length	Diameter	Scale	Statistics	Length	Diameter	Scale	Statistics	Statistics	Statistics	Statistics
1	1.219	1.219	1.034	1.162	1.223	1.223	1.043	1.168	0.380	2.435	2.423	2.010
2	1.102	1.102	1.045	1.087	1.109	1.109	1.066	1.086	0.510	2.290	2.189	1.837
3	1.166	1.166	1.004	1.050	1.177	1.177	1.010	1.055	0.410	2.309	2.323	1.686
4	1.081	1.081	0.966	1.038	1.100	1.100	0.988	1.013	0.889	2.377	2.152	1.704
5	0.999	0.988	0.904	0.999	1.018	1.018	0.915	0.948	0.580	2.189	1.963	1.616
6	0.934	0.898	0.835	0.934	0.925	0.925	0.846	0.877	0.470	1.980	1.793	1.509
7	0.969	0.962	0.914	0.969	1.004	1.004	0.937	0.923	0.464	2.165	1.883	1.615
8	1.266	1.187	1.088	1.266	1.159	1.119	1.084	1.159	0.806	2.895	2.316	2.443
9	1.171	1.148	1.000	1.171	1.081	1.081	1.030	1.061	0.223	2.647	2.249	2.905
10	1.131	1.081	0.969	1.131	1.032	1.032	1.005	1.028	0.938	2.533	2.119	3.212
11	1.503	1.503	0.885	1.091	1.348	1.348	0.955	1.050	1.929	2.677	2.862	**3.509**
12	1.379	1.379	0.955	1.038	1.242	1.242	1.051	0.996	2.962	2.579	2.633	3.185
13	1.478	1.478	0.932	1.179	1.297	1.297	0.995	1.115	1.550	2.931	2.880	**3.445**
14	1.396	1.396	0.841	1.124	1.221	1.221	0.901	1.121	0.680	2.778	2.707	3.242
15	1.403	1.403	0.861	1.177	1.300	1.300	0.941	1.191	1.875	2.967	2.730	3.224
16	∞	∞	0.837	∞	∞	**1.930**	0.913	∞	6.737	3.087	**4.407**	**3.418**
17	∞	∞	1.002	∞	∞	**2.075**	1.042	∞	9.225	3.089	**4.571**	**3.446**
18	∞	∞	0.963	∞	∞	**1.911**	0.978	∞	5.832	3.088	**4.155**	**3.433**
19	∞	∞	1.019	∞	∞	1.789	1.033	∞	8.793	2.850	**3.872**	3.162
20	∞	∞	1.140	∞	∞	1.685	1.163	∞	7.408	2.704	**3.576**	3.092
21	∞	∞	1.625	∞	∞	1.595	1.612	∞	5.077	2.531	**3.367**	3.243
22	∞	∞	1.642	∞	∞	1.478	1.637	∞	3.947	2.309	3.110	3.119
23	∞	∞	**1.905**	∞	∞	1.556	1.865	∞	8.434	2.474	3.242	2.815
24	∞	∞	**2.226**	∞	∞	1.441	**2.149**	∞	12.412	2.397	3.003	2.848
25	∞	∞	**2.379**	∞	∞	1.324	**2.289**	∞	**24.041**	2.520	2.767	2.670
26	∞	∞	**2.514**	∞	∞	1.195	**2.429**	∞	**22.137**	2.513	2.490	2.427
27	∞	∞	**2.449**	∞	∞	1.104	**2.378**	∞	**23.602**	2.545	2.320	2.637
28	∞	∞	**2.269**	∞	∞	1.007	**2.228**	∞	**28.388**	2.304	2.166	2.390
29	∞	∞	**2.078**	∞	∞	1.036	**2.049**	∞	19.708	2.132	2.180	2.166
30	∞	∞	**1.911**	∞	∞	1.019	**1.901**	∞	17.885	2.079	2.127	2.068
31	∞	∞	**2.158**	∞	∞	0.941	**2.038**	∞	20.390	2.152	1.968	2.361
32	∞	∞	∞	∞	∞	0.979	∞	∞	**37.607**	**5.094**	3.140	**5.361**
33	∞	∞	∞	∞	∞	1.341	∞	∞	**36.335**	**9.861**	**5.781**	**10.174**
34	∞	∞	∞	∞	∞	∞	∞	∞	**55.366**	**14.206**	**9.105**	**14.506**

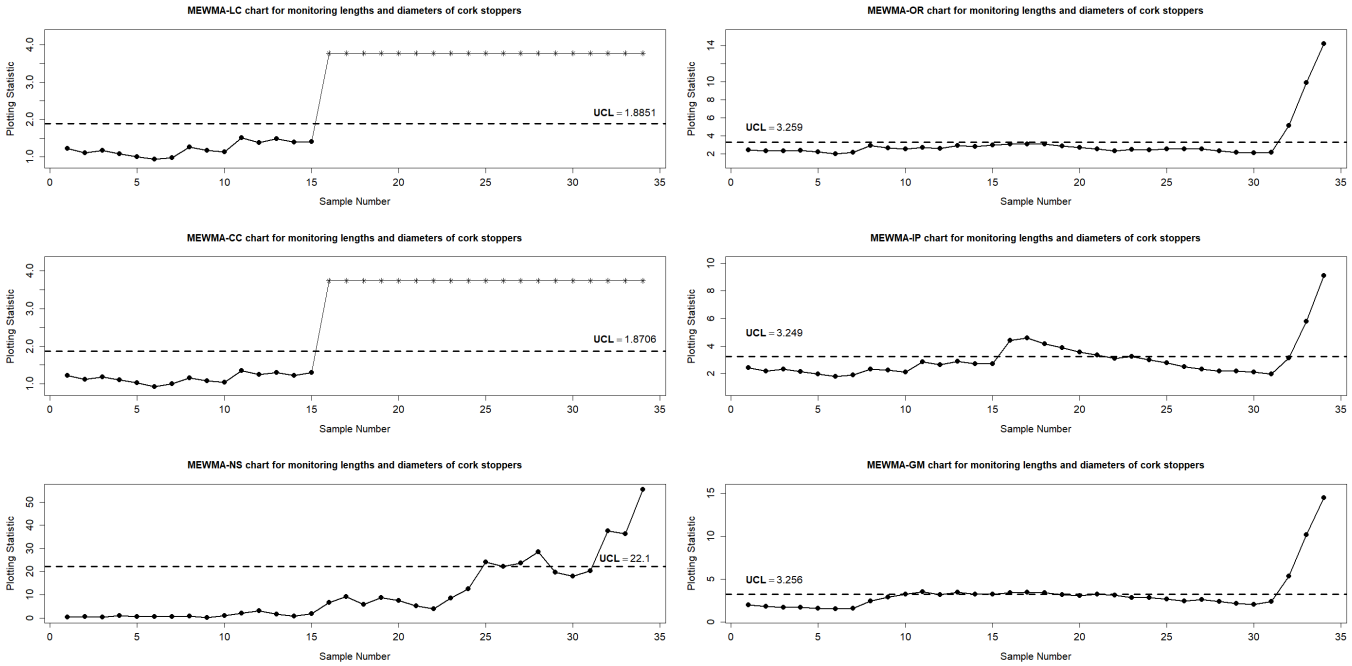

Figure 12: Six schemes for monitoring and diagnosis of corks' lengths and diameters. Note: the plotting statistics of the Phase-II MEWMA-LC and MEWMA-CC schemes can theoretically be infinity and thus any value greater than twice the UCL is shown by an asterisk at the $2 \times UCL$, while exact values are shown with a solid point.

Appendix

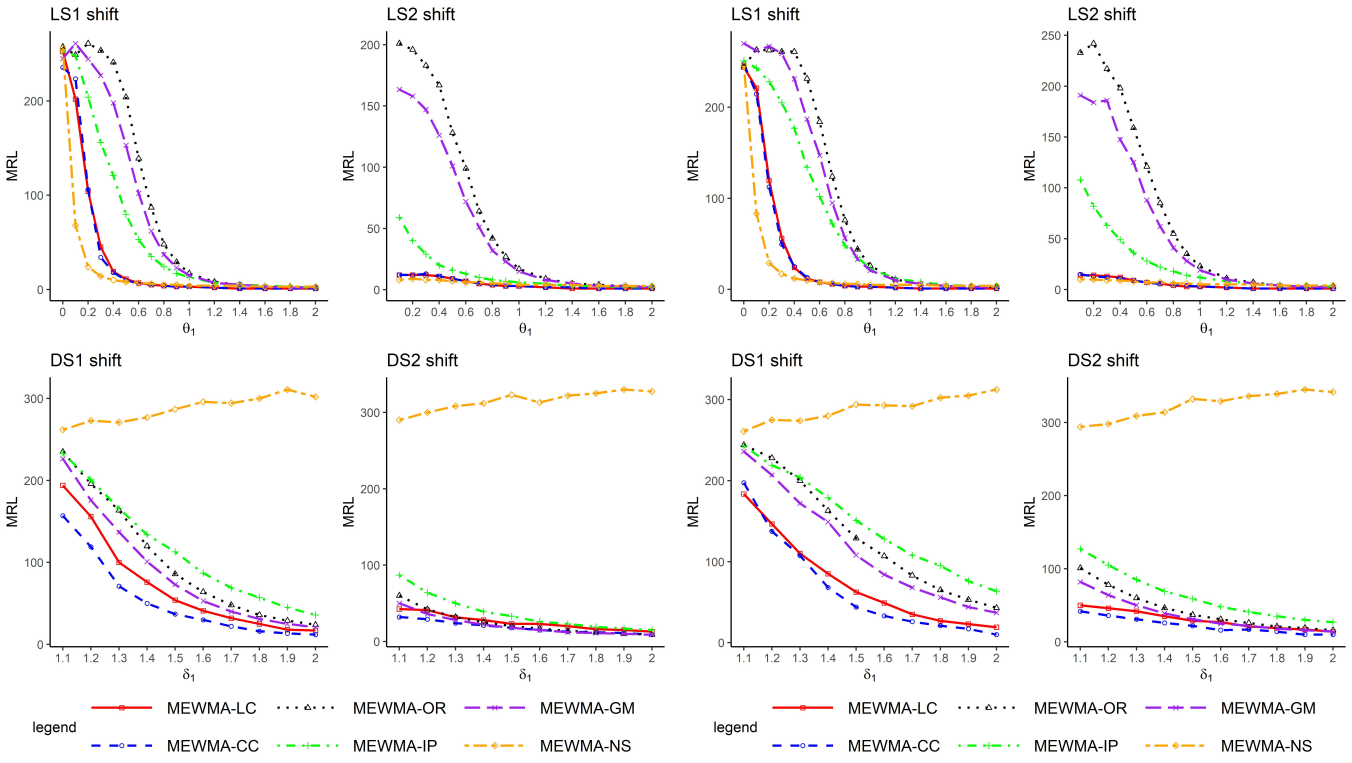

(a) $d = 2$ (b) $d = 3$

Figure A1: OOC performance comparisons of six multivariate EWMA schemes under d-variate **t(3)** distribution for **LS and DS shifts** with $m = 100, n = 15, \boldsymbol{\lambda = 0.1}$ and the target $\text{MRL}_0 = 250$. Note that the figures in the first and second columns are for $d = 2$ and the figures in the third and fourth columns are for $d = 3$. The first row is OOC performance under shift situation-LS and the second row is OOC performance under shift situation-DS.

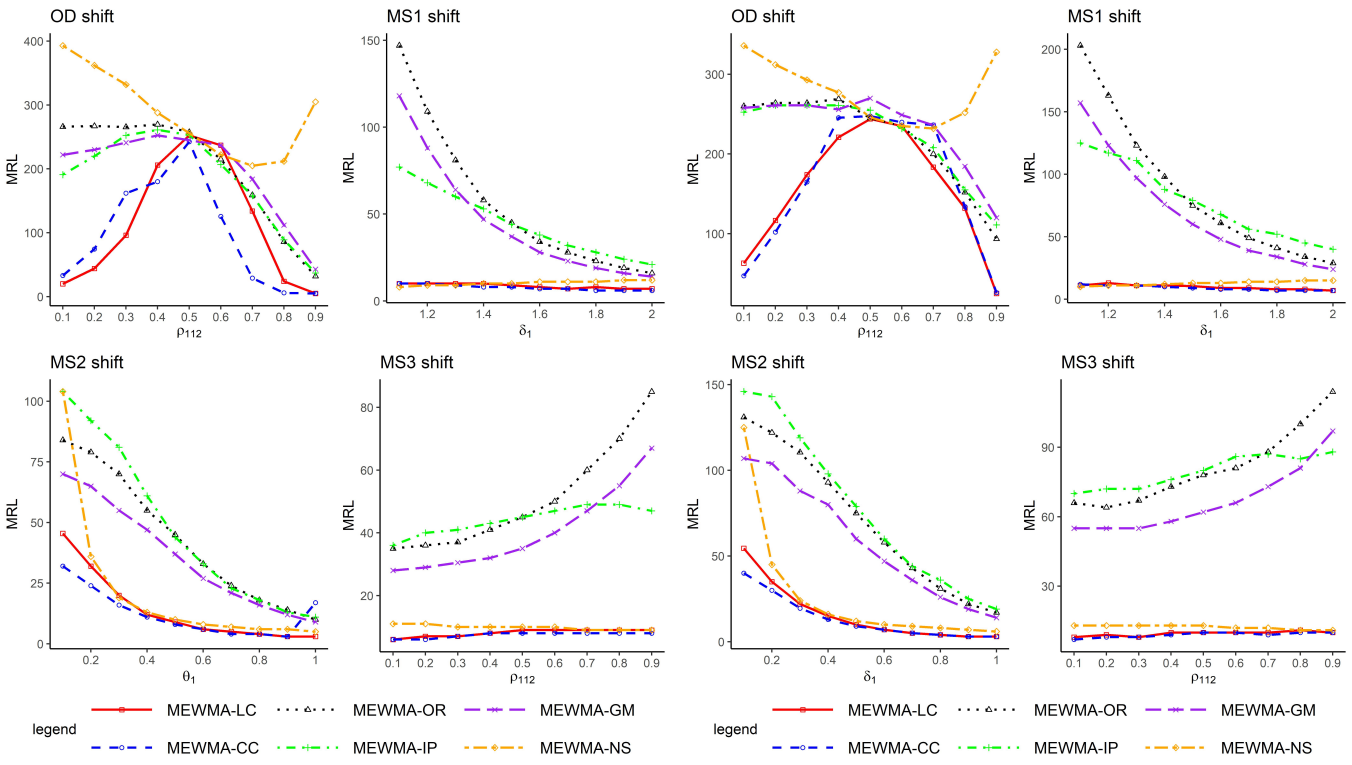

(c) $d = 2$ (d) $d = 3$

Figure A2: OOC performance comparisons of six multivariate EWMA schemes under d-variate **t(3)** distribution for **OD and MS shifts** with $m = 100, n = 15, \boldsymbol{\lambda = 0.1}$ and the target $\text{MRL}_0 = 250$. Note that the figures in the first and second columns are for $d = 2$ and the figures in the third and fourth columns are for $d = 3$. The first figure in the first row is OOC performance under shift situation-OD and the others are OOC performance under shift situation-MS.

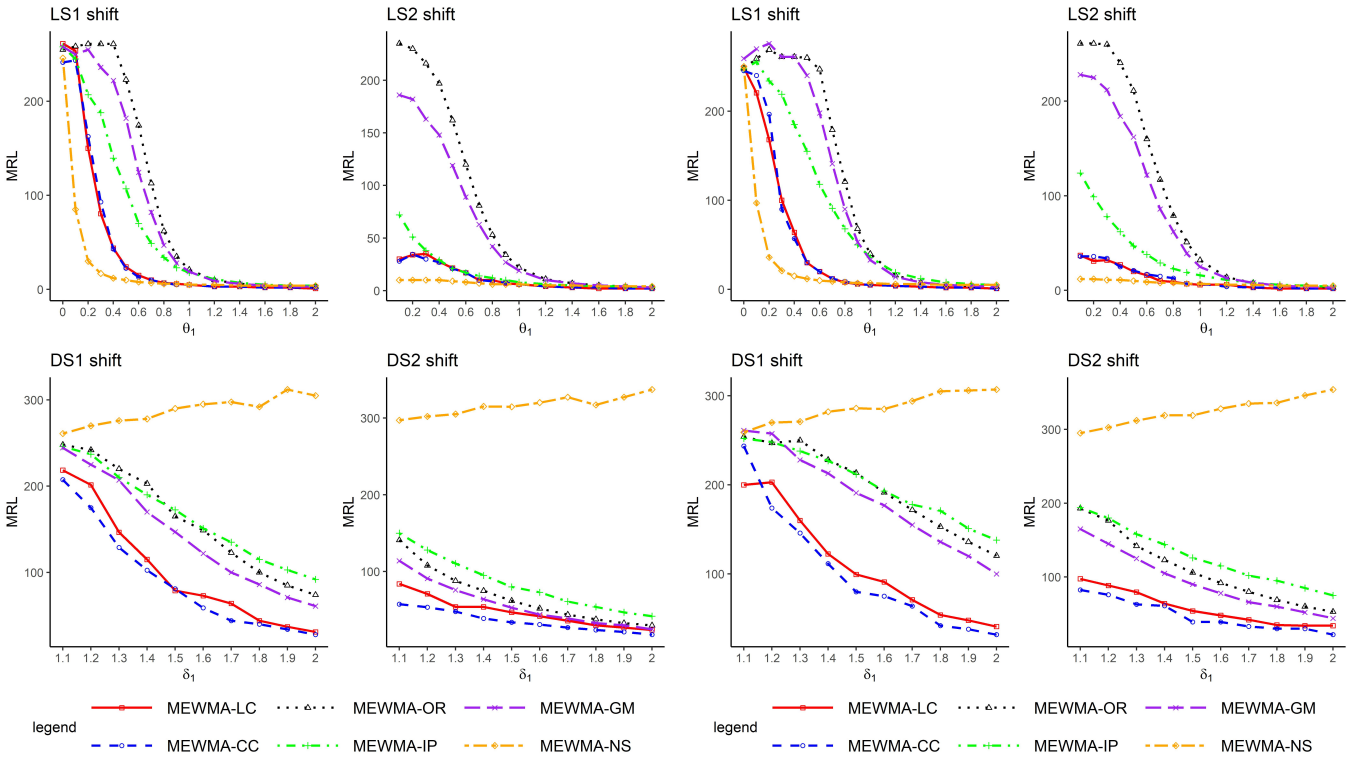

(e) $d = 2$ (f) $d = 3$

Figure A3: OOC performance comparisons of six multivariate EWMA schemes under d-variate **Cauchy** distribution for **LS and DS shifts** with $m = 100, n = 15, \boldsymbol{\lambda = 0.1}$ and the target $\text{MRL}_0 = 250$. Note that the figures in the first and second columns are for $d = 2$ and the figures in the third and fourth columns are for $d = 3$. The first row is OOC performance under shift situation-LS and the second row is OOC performance under shift situation-DS.

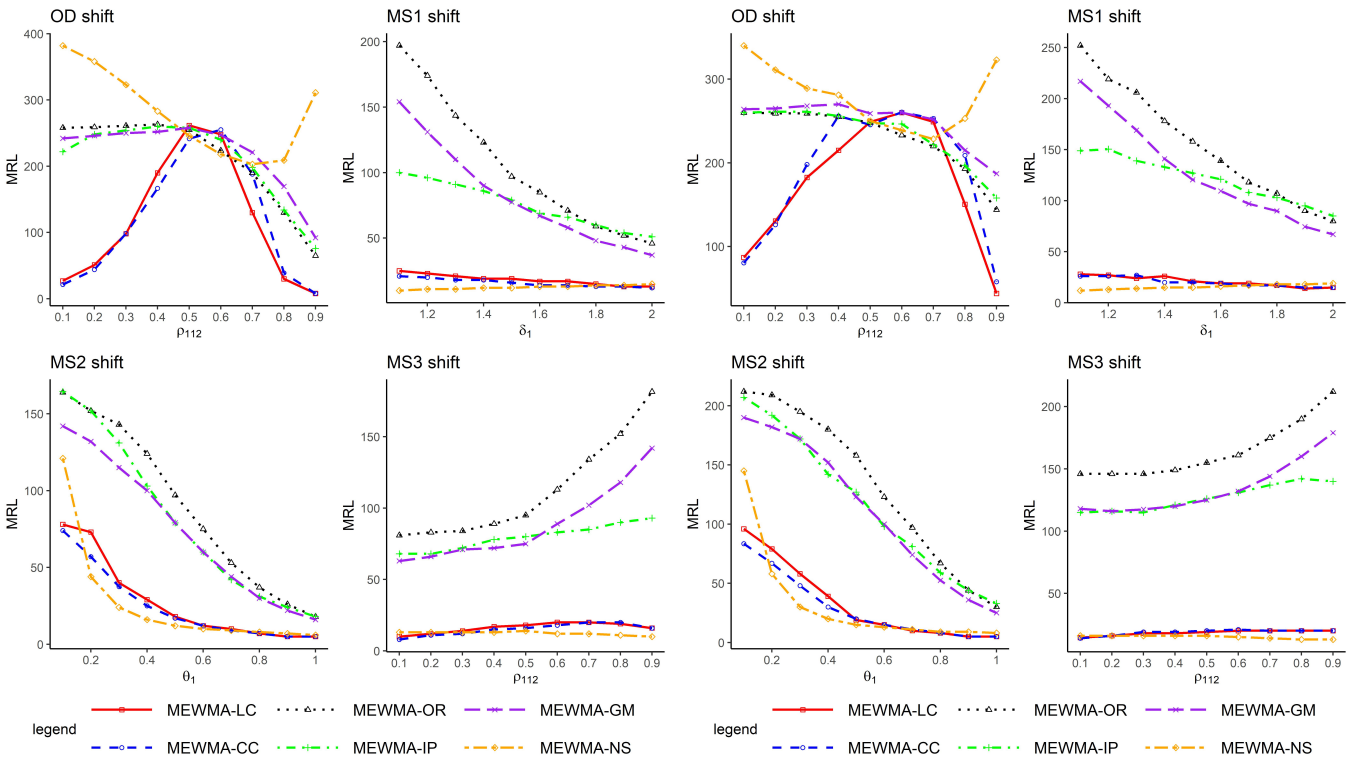

(g) $d = 2$ (h) $d = 3$

Figure A4: OOC performance comparisons of six multivariate EWMA schemes under d-variate **Cauchy** distribution for **OD and MS shifts** with $m = 100, n = 15, \boldsymbol{\lambda = 0.1}$ and the target $\text{MRL}_0 = 250$. Note that the figures in the first and second columns are for $d = 2$ and the figures in the third and fourth columns are for $d = 3$. The first figure in the first row is OOC performance under shift situation-OD and the others are OOC performance under shift situation-MS.

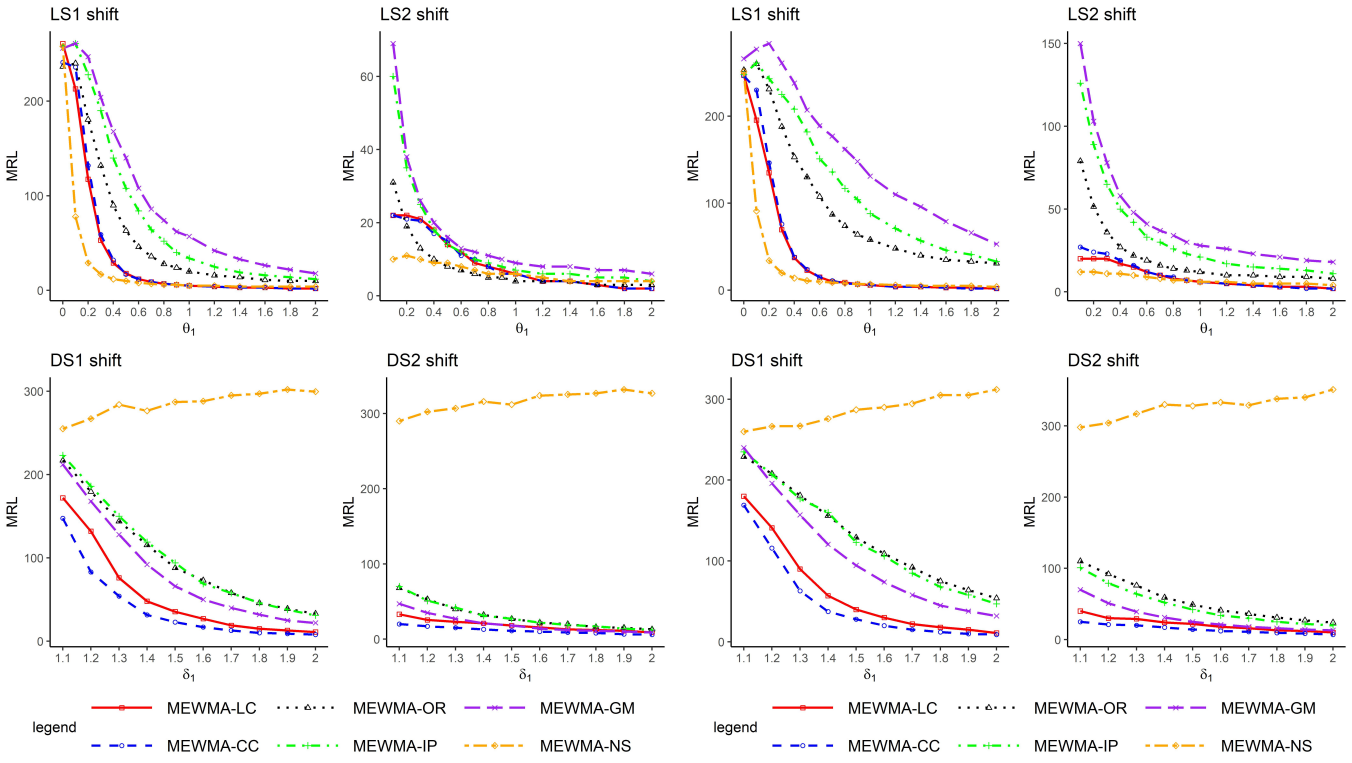

(i) $d = 2$ (j) $d = 3$

Figure A5: OOC performance comparisons of six multivariate EWMA schemes under d-variate **exponential** distribution for **LS and DS shifts** with $m = 100, n = 15, \boldsymbol{\lambda = 0.1}$ and the target $\text{MRL}_0 = 250$. Note that the figures in the first and second columns are for $d = 2$ and the figures in the third and fourth columns are for $d = 3$. The first row is OOC performance under shift situation-LS and the second row is OOC performance under shift situation-DS.

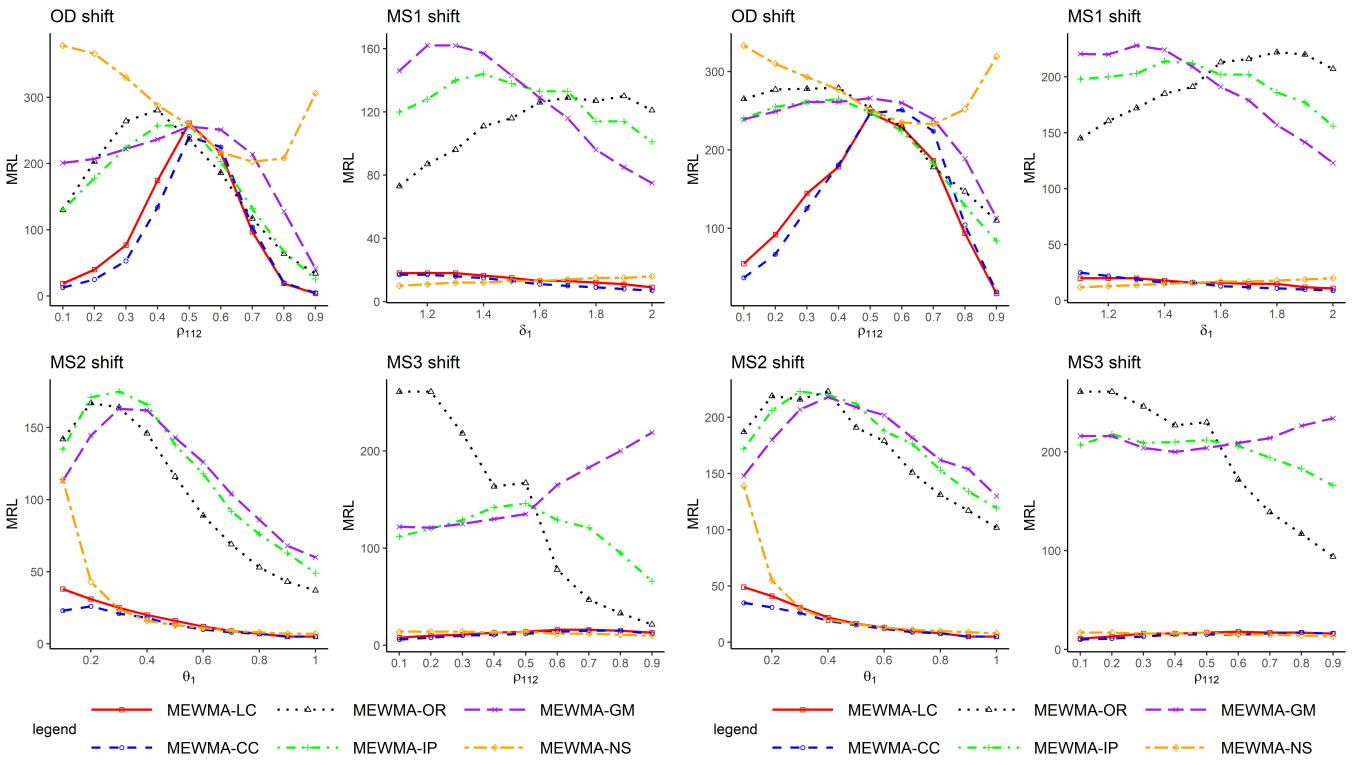

(k) $d = 2$ (l) $d = 3$

Figure A6: OOC performance comparisons of six multivariate EWMA schemes under d-variate **exponential** distribution for **OD and MS shifts** with $m = 100, n = 15, \boldsymbol{\lambda = 0.1}$ and the target $\text{MRL}_0 = 250$. Note that the figures in the first and second columns are for $d = 2$ and the figures in the third and fourth columns are for $d = 3$. The first figure in the first row is OOC performance under shift situation-OD and the others are OOC performance under shift situation-MS.

References

[1] Qiu, P. (2014), *Introduction to Statistical Process Control*, Boca Raton, FL: Chapman Hall/CRC.

[2] Shewhart, W.A. (1931), *Economic Control of Quality of Manufactured Product*, New York: D. Van Nostrand Company.

[3] Song, Z., Mukherjee, A., and Tao, G. (2020), "A class of distribution-free one-sided Cucconi schemes for joint surveillance of location and scale parameters and their application in monitoring cab services," *Computers & Industrial Engineering*, DOI: 10.1016/j.cie.2020.106625.

[4] Mukherjee, A., and Marozzi, M. (2017), "A distribution-free phase-II CUSUM procedure for monitoring service quality," *Total Quality Management Business Excellence*, **28**, 1227-1263.

[5] Zhang, T., He, Z., Zhao, X., and Qu L. (2021), "Joint monitoring of post-sales online review processes based on a distribution-free EWMA scheme," *Computers & Industrial Engineering*, DOI: 10.1016/j.cie.2021.107372.

[6] Qiu, P., and Hawkins, D.M. (2001), "A rank based multivariate CUSUM procedure," *Technometrics*, **43**, 120-132.

[7] Qiu, P., and Hawkins, D.M. (2003), "A nonparametric multivariate CUSUM procedure for detecting shifts in all directions," *JRSS-D (The Statistician)*, **52**, 151-164.

[8] Qiu, P. (2008), "Distribution-free multivariate process control based on log-linear modeling," *IIE Transactions*, **40**, 664-677.

[9] Liu, L., Tsung, F., and Zhang, J. (2014), "Adaptive nonparametric CUSUM scheme for detecting unknown shifts in location," *International Journal of Production Research*, **52**, 1592-1606.

[10] Qiu, P., and Zhang, J. (2015), "On phase II SPC in cases when normality is invalid," *Quality and Reliability Engineering International*, **31**, 27-35.

[11] Hou, S., and Yu, K. (2020), "A nonparametric CUSUM control chart for process distribution change detection and change type diagnosis," *International Journal of Production Research*, 1-21.

[12] Qiu, P. (2018), "Some Perspectives On Nonparametric Statistical Process Control," *Journal of Quality Technology*, **50**, 49-65.

[13] Chakraborti, S., and Graham, M.A. (2019), "Nonparametric (distribution-free) control charts: An updated overview and some results," *Quality Engineering*, **31**, 523-544.

[14] Li, J., Jeske, D.R., Zhou, Y., and Zhang, X. (2019), "A wavelet-based nonparametric CUSUM control chart for autocorrelated processes with applications to network surveillance," *Quality and Reliability Engineering International*, **5**, 644-658.

[15] Qiu, P. (2020), "Big data? Statistical process control can help!" *The American Statistician*, **74**, 329-344.

[16] Mukherjee, A., and Marozzi, M. (2020), "Nonparametric Phase-II control charts for monitoring high-dimensional processes with unknown parameters," *Journal of Quality Technology*, DOI: 10.1080/00224065.2020.1805378

[17] Xue, L., and Qiu, P. (2021), "A nonparametric CUSUM chart for monitoring multivariate serially correlated processes," *Journal of Quality Technology*, **53**, 396-409.

[18] Song, Z., Mukherjee, A., and Zhang, J. (2021), "Some robust approaches based on copula for monitoring bivariate processes and component-wise assessment," *European Journal of Operational Research*, **289**, 177-196.

[19] Tran K.P. (2022) *Control Charts and Machine Learning for Anomaly Detection in Manufacturing, Springer Series in Reliability Engineering*. Cham: Springer.

[20] Qiu, P., and Xie, X. (2021), "Transparent sequential learning for statistical process control of serially correlated data," *Technometrics*, DOI: 10.1080/00401706.2021.1929493.

[21] Zou, C., Wang, Z., and Tsung, F. (2012), "A spatial rank-based multivariate EWMA control chart," *Naval Research Logistics*, **59**, 91-110.

[22] Li, Z., Zou, C., Wang, Z., and Huwang, L. C. (2013), "A multivariate sign chart for monitoring process shape parameters," *Journal of Quality Technology*, **45**, 149-165.

[23] Chen, N., Zi, X., and Zou, C. (2016), "A distribution-free multivariate control chart," *Technometrics*, **58**, 448-459.

[24] Jones-Farmer, L. A., Woodall, W. H., Steiner, S. H., and Champ, C. W. (2014). "An overview of phase I analysis for process improvement and monitoring," *Journal of Quality Technology*, **46**, 265-280.

[25] Capizzi, G., and Masarotto, G. (2018), *Phase-I distribution-free analysis with the R package dfphase1, Frontiers in statistical quality control: 12*. Cham: Springer.

[26] Sklar, A. (1959), "Fonctions de répartition à n dimensions et leurs marges," *Publications de l'Institut de Statistique de l'Université de Paris*, **8**, 229-231.

[27] Marozzi, M. (2013), "Nonparametric simultaneous tests for location and scale testing: a comparison of several methods," *Communications in Statistics-Simulation and Computation*, **42**, 1298-1317.

[28] Nishino, T., and Murakami, H. (2019), "The Cucconi statistic for Type-I censored data," *Metrika*, **82**, 903-929.

[29] Song, Z., Mukherjee, A., Marozzi, M., and Zhang, J. (2020), *A class of distribution-free exponentially weighted moving average schemes for joint monitoring of location and scale parameters*, In Distribution-free Methods for Statistical Process Monitoring and Control. Editors: Koutras, Markos V., Triantafyllou, Ioannis S., Switzerland AG: Springer Nature.